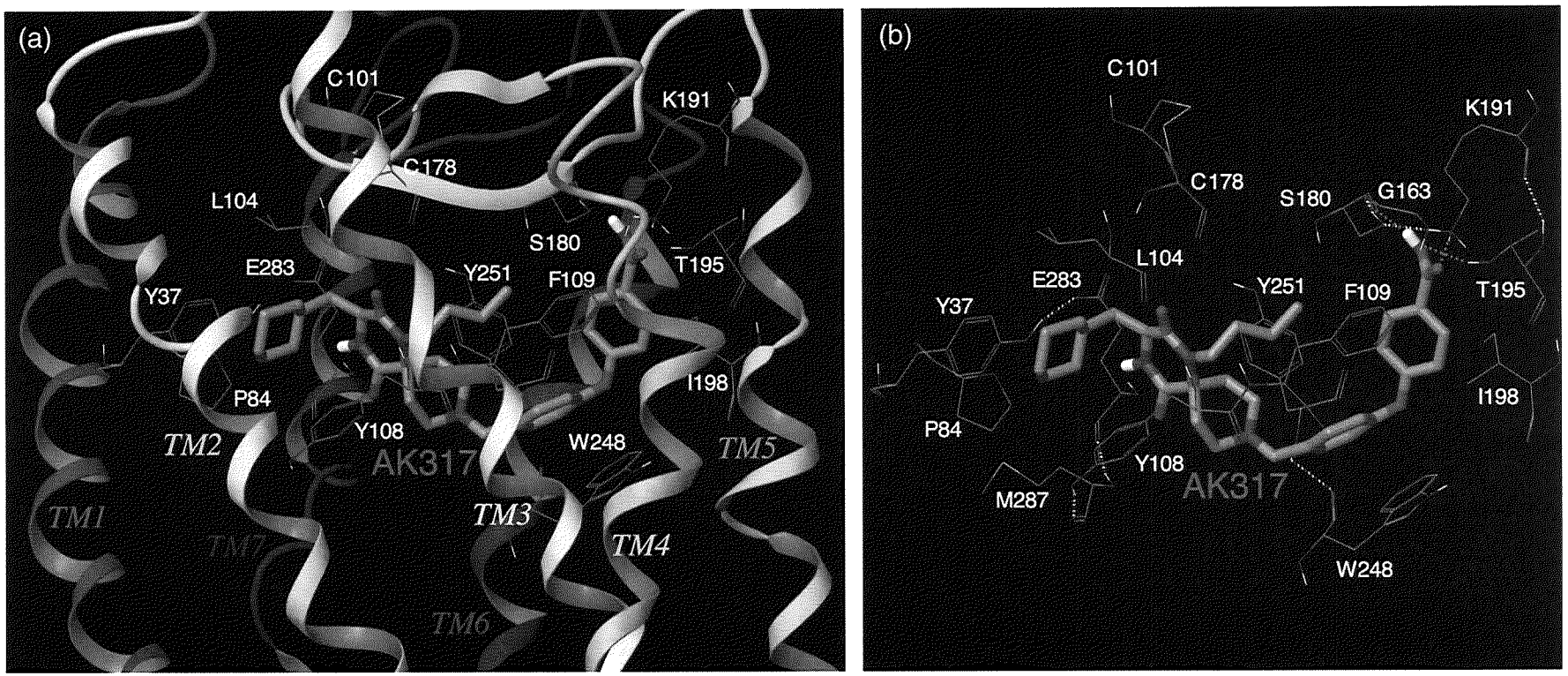


**Fig. 6.** Amino acid residues forming the binding cavity within CCR5 for AK317. (a) The binding mode of AK317 within CCR5 is shown. (b) The intramolecular hydrogen bond interactions of CCR5 defining the binding cavity and the binding interactions of AK317 with CCR5 are shown. AK317 has hydrogen bond interactions with S180, K191, and T195 (pink dotted line). Other residues in the binding cavity are predicted to have hydrophobic interactions with AK317. As in the case of AK530, there are several intramolecular hydrogen bond networks (yellow dotted line) that define the shape of the CCR5 binding cavity for AK317. There is a network involving S180(ECL2), G163(TM4), K191(TM5), and T195(TM5), and another network involving Y37(TM1), E283(TM7), M287(TM7), and Y108(TM3). The conformation involving amino acid residues in the latter network differs from that of the case of AK530 binding. It appears that CCR5 undergoes different conformational changes to accommodate different inhibitors.

TM6. The phenoxy-benzoic acid group of AK317 interacts with S180 and K191. S180 is a part of ECL2, whereas K191 in TM5 is likely located above the plane of the extracellular region. The pyrazol group of AK530, on the other hand, bends towards the cytoplasmic region and makes the inhibitor bind deeper into the cavity. There are no direct interactions of AK530 with K191, but it seems to be forming a favorable conformation of the binding pocket by an intramolecular hydrogen bond network with G163 and T195 (Fig. 5c). K191, located in the upper domain of TM5, can be considered to be an extracellular residue as well, since a part of K191 is located above the cellular plane (Fig. 2). We speculate that the direct interactions of AK317 with the ECL2 residues such as S180 and with the residues in the extracellular region (such as K191) are responsible for its high antiviral $IC_{50}$ of 2 nM (Table 1). In spite of being a weaker binder compared to AK530, the interactions of the phenoxy-benzoic acid group of AK317 seem to be responsible for its comparable antiviral potency with AK530, which has no direct interaction with ECL2 residues in the vicinity of TM4 and TM5.

The binding cavities of both AK530 and AK317 are mostly lipophilic (Fig. 4a and b). The only strongly hydrophilic regions are towards the extracellular loop region. The shape and volume of the cavities are slightly different for these two inhibitors, as CCR5 is likely to undergo conformational changes to different extents to accommodate these two inhibitors. The unoccupied regions of the cavity suggest new optimization ideas for these inhibitors. For example, substituents of AK530 that can potentially interact with K191 may increase its antiviral potency even further.

### Determination of interatomic distances between key amino acids when AK317 and AK530 bind to CCR5

In an attempt to examine whether the binding of AK317 or AK530 to CCR5 causes significant changes in interatomic distances between key amino acids that form the hydrogen bond network seen in the unbound CCR5 as described above (Fig. 3), we carried out molecular dynamics simulation for 4800 ps for AK317- and AK530-bound CCR5, and analyzed critical interatomic distances with the unbound conformation (Fig. 7a–c). In the unbound conformation, Y108 in TM3 was in close proximity to Y251 located in TM6 and had a hydrogen bond interaction with E283 in TM7 (Figs. 3 and 7a and b). In the AK317-bound CCR5, Y108 had rotated away from Y251, and the hydrogen bond interaction between Y108 and E283 was lost. Rotation of Y108 away from Y251 and disruption of hydrogen bond interaction between Y108 and E283 were also observed when AK530 bound to CCR5. TM2 and TM3 can be thought to be in a single plane (above the plane of the paper), and TM6 and TM7 can be thought to be in a different plane (behind the plane of the paper). The rearrangement of Y108 was necessary for the formation of the binding cavity between the transmembrane helices for inhibitor binding. Furthermore, in the unbound CCR5 structure, E283 is hydrogen-bonded to S180, which is part of the ECL2 (Fig. 3). In fact, E283 moved considerably away from S180 in the inhibitor-bound models of CCR5 (Figs. 5c, 6b, and 7c). Disruption of hydrogen bonds between transmembrane residues and a network of hydrogen bonds mediated through water molecules are known to give rise to the change in the intracellular loop conformation of bovine rhodopsin.[29,30] Change in ionic interactions between transmembrane residues is also thought to be responsible for the activation of $\beta_2$-adrenergic receptor.[34] We speculate that the rotation of Y108 away from the vicinity of Y251, the loss of hydrogen bond interaction between Y108 and E283, and the loss of hydrogen bond interaction between E283 and S180 presumably change the conformation of the ECL2 that is crucial for the binding of the gp120/CD4 complex. These models of unbound and inhibitor-bound CCR5 may give further insights into the mechanism of the inhibition of CCR5 inhibitors involving transmembrane and extracellular residues interacting with each other.

### Structural changes in ECL2 caused by CCR5 inhibitors block the binding of CCR5-specific monoclonal antibodies to CCR5

Our structural analyses described above demonstrated that AK530 relatively well maintained its CCR5 binding with the K191A substitution, while AK317 significantly reduced its interactions with $CCR5_{K191A}$, prompting us to examine whether the different CCR5-binding profiles of these two inhibitors led to different dynamics in their interactions with CCR5-specific monoclonal antibodies (mAbs). To this end, we examined whether AK530 and AK317 blocked the binding to CCR5 expressed on CHO cells of four mAbs: 45531 [specific for the C-terminal half of ECL2 (ECL2B)], 45523 (reactive to CCR5 multidomain), 2D7 [specific for the N-terminus of ECL2 (ECL2A)], and 45549 (reactive to CCR5 multidomain).[25,35,36] In this mAb-binding blocking assay, the cells were incubated with each inhibitor for 30 min, followed by the addition of a mAb. As shown in Fig. 8, AK317 effectively inhibited the binding of mAb 45531 with an $IC_{50}$ value of 16.3 nM, while the inhibition by AK530 was much less, with an $IC_{50}$ value of 746 nM. AK317 also blocked the binding of mAb 45523 with an $IC_{50}$ value of 282 nM, while AK530 did so with an $IC_{50}$ value of $>1$ μM. None of the inhibitors blocked the binding of mAb 2D7 or 45549. When the cells were first exposed to a mAb, followed by the addition of each inhibitor, the resultant inhibition levels were virtually the same (data not shown). Considering that these CCR5 inhibitors are lodged in a hydrophobic pocket at the interface of ECL2 and the upper transmembrane domain (Figs. 4–6), the observed inhibition of mAb binding by CCR5 inhibitors presumably occurred through the allosteric changes secondarily caused by CCR5 binding of the inhibitor, but not through their competition over binding to the antigenic epitope (s) of CCR5.

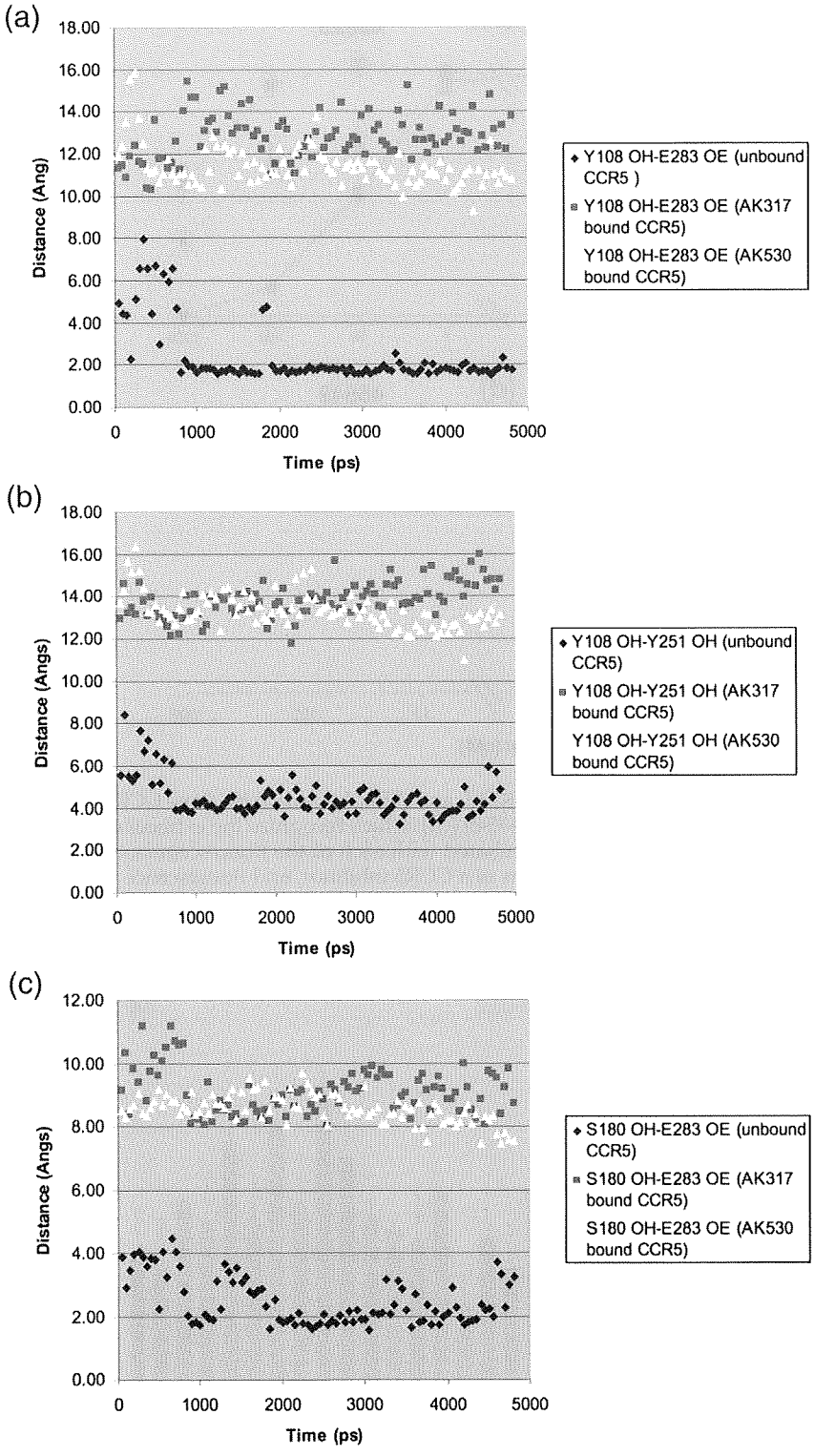


**Fig. 7.** Key interatomic distances from molecular dynamics simulation of AK317-bound, AK530-bound, and unbound CCR5. Molecular dynamics simulation for AK317- and AK530-bound CCR5 was conducted for 4800 ps, and critical interatomic distances between key amino acids were determined. A hydrogen bond is present if the interatomic distance is <3 Å. (a) Distance between Y108 (hydroxyl hydrogen, PDB atom-type OH) and E283 (carboxylate oxygen, PDB atom-type OE). In the unbound conformation, there is a strong hydrogen bond interaction between Y108 in TM3 and E283 in TM7. Y108 and E283 have to move away from each other to form the binding cavity for the inhibitor to bind, and there is no hydrogen bond between these residues after AK317 and AK530 binding. (b) Distance between Y108 and Y251 hydroxyl oxygen: the tyrosines have moved away from each other after inhibitor binding. (c) Distance between E283 (carboxylate oxygen, PDB atom-type OE) and S180 (hydroxyl hydrogen, PDB atom-type OH). In the unbound conformation, E283 in TM7 has hydrogen bond interactions with S180 in ECL2. This hydrogen bond is disrupted for AK317- and AK530-bound CCR5.

### Effects of amino acid substitutions in CCR5 on HIV-1-gp120-elicited cell fusion

In order to better understand conformational changes arising in ECL2 and to determine amino acids that are critical for the cellular entry of HIV-1, we examined the effects of single and multiple amino acid substitutions in ECL2 on HIV-1-gp120-elicited cell fusion. Figure 9 shows the magnitude of cell–cell fusion between $tat^+$,$env^+$ 293T cells and $Luc^+$,$CCR5^+$ MAGI cells in the HIV-1-gp120-elicited cell–cell fusion assay. Seven single amino acid substitutions introduced into CCR5 resulted in a substantial reduction (>70%) in the HIV-1-envelope-protein-elicited fusion level (Fig. 9). Three of these single amino acid substitutions (E172A, L174A, and C178A) are located in the ECL2 with an antiparallel β-hairpin structure, while C101A and G163R are in TM3 and TM4, respectively,

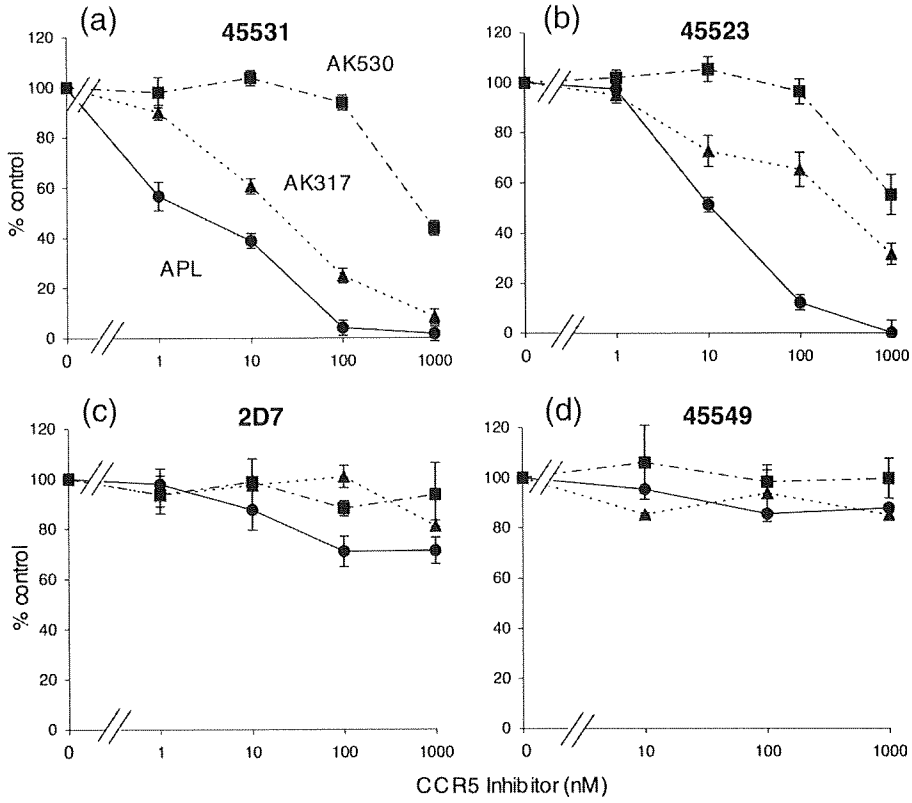


**Fig. 8.** Inhibition of the binding of anti-CCR5 mAbs by AK530, AK317, and APL. Inhibition by three CCR5 inhibitors of the binding of anti-CCR5 mAbs [45531 (a), 45523 (b), 2D7 (c), and 45549 (d)], which recognize the extracellular domain (s) of CCR5, is illustrated. CCR5-overexpressing CHO cells were incubated with each of the fluorescein-isothiocyanate-conjugated anti-CCR5 mAbs in the presence of various concentrations of a CCR5 inhibitor, and fluorescence intensity on the cells was determined. Each value was compared to that obtained without an inhibitor and is shown as percent control.

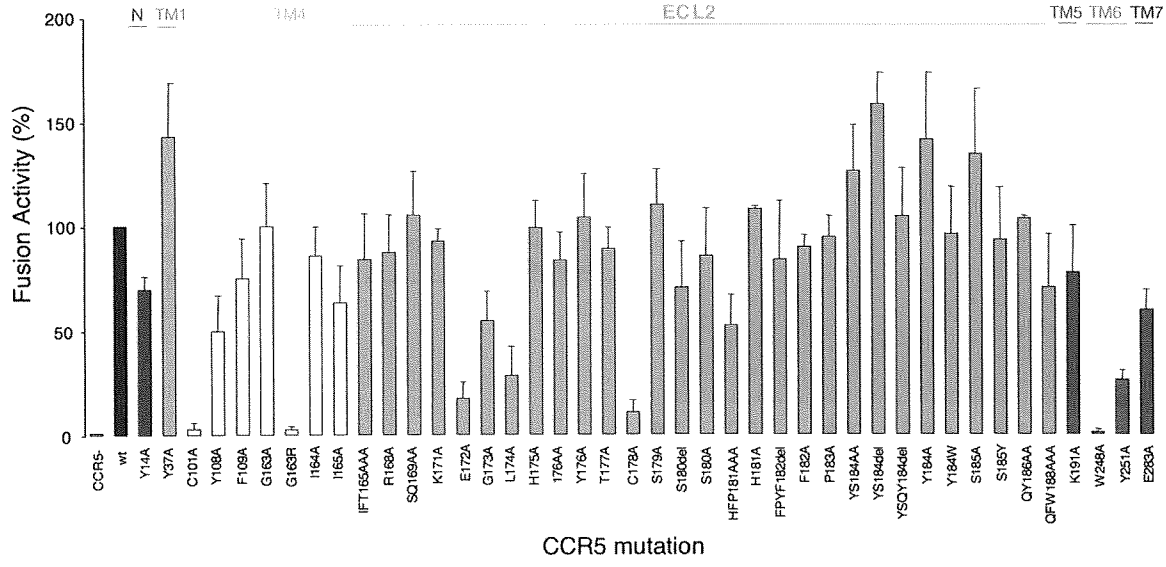


**Fig. 9.** Effects of amino acid substitution(s) and deletion(s) on HIV-1-gp120-elicited cell–cell fusion. $CD4^+$ MAGI cells that expressed sufficient numbers of wild-type or mutated CCR5 were cultured with HIV-1 $env^+$, $tat^+$ 293T cells for 6 h, and fusion efficiency was determined with luciferase activity (luminescence levels) using the reporter gene activation assay. The magnitude of luminescence levels with mutant CCR5 is expressed as percent fusion (percent control compared to the luminescence level with wild-type CCR5). Note that three single amino acid substitutions (E172A, L174A, and C178A), which resulted in a substantial reduction in the fusion level (>70%), are located in the ECL2 that has an antiparallel β-hairpin structure (Figs. 2 and 3), while C101A and G163R are in TM3 and TM4, respectively, and W248A and Y251A are in TM6.

and W248A and Y251A are in TM6 (Figs. 2 and 3). Note that E172 is at the $NH_2$ end of the β-sheet structure of ECL2 and that C178 also belongs to the β-hairpin structural motif (Fig. 2). This finding strongly suggests that these mutations led to the disruption of ECL2's β-sheet structure and resulted in a significant reduction in the cell–cell fusion. Thus, the β-sheet structure of ECL2 seems to be critical for the cellular entry of HIV-1. It is noteworthy that although the two amino acids E172 and L174 do not interact with CCR5 inhibitors (Figs. 4–6), their mutations significantly reduced cell–cell fusion (Fig. 9).

The C101A and C178A substitutions are thought to disrupt the disulfide bond between C101 and C178, which is crucial for the maintenance of the robust ECL2 structure, as demonstrated in this study. Thus, both C101A and C178A substitutions probably led to the aborted HIV-1-envelope-elicited fusion. G163, located in TM4, does not interact directly with AK530, AK317, or APL, but is responsible for maintaining the shape of the binding cavity by its hydrogen bond interactions with S180, K191, and T195 (Figs. 5 and 6). G163R substitution also resulted in virtually a complete loss of fusion (Fig. 9). This is consistent with earlier observations that G163R mutation results in the loss of HIV-1 infectivity.[22,31]

Amino acids within ECL2 at positions 179 through 190 appeared not to have a crucial role in the HIV-1-envelope-elicited fusion. Indeed, the amino acid substitutions in these positions did not significantly reduce the fusion (Fig. 9). It is noteworthy that these amino acids are located distant from the binding cavity for CCR5 inhibitors (Figs. 2, 5, and 6). It is also of note that W248 has hydrogen bond interactions with Y251 and is thought to play a role in maintaining the conformation of ECL2 (Fig. 3), explaining the reason that W248A substitution results in loss of fusion.

Interestingly, both C178A and C101A substitutions substantially reduced CCR5 binding of the three CCR5 inhibitors (AK530, AK317, and APL), but not that of SCH-C or TAK-779.[22] In particular, APL forms hydrogen bonds with C178 and, additionally, has tight interactions with the intramolecular hydrogen bond network (S180/G163/K191/T195).[22] AK317 also has interactions with the S180/G163/K191/T195 network (Fig. 6). Thus, SDP-containing CCR5 inhibitors, especially APL and AK317, appear to have greater interactions with ECL2 compared to other non-SDP-containing CCR5 inhibitors such as SCH-C or TAK-779. Our observation that AK530 has the greatest binding affinity for CCR5 (Table 1) but exerts less potent anti-HIV-1 activity (Table 1) may be related to its reduced interactions with ECL2 (Figs. 5 and 7). Such tight interactions with ECL2 may represent a feature conferring potent anti-HIV-1 activity on CCR5 inhibitors, different from allosteric changes caused by CCR5 inhibitors.

## Discussion

In the present study, we demonstrated that two novel CCR5 inhibitors, AK530 and AK317, are lodged in a hydrophobic cavity located between the upper transmembrane domain and ECL2. CCR5 is a member of GPCRs, the largest superfamily of proteins in the body. Understanding the structure of human GPCRs would be invaluable in elucidating their roles in a number of biological processes and should also greatly aid in designing therapeutics. In particular, the elucidation of the detailed structure of human CCR5 and its interactions with HIV-1 envelope glycoprotein should help establish a strategy for HIV-1 intervention. However, no crystal structures of human CCR5 are yet available; bovine rhodopsin and $\beta_2$-adrenergic receptors are the only GPCR species for which crystallographic data have been obtained.[32,37] Thus, we have previously explored an alternate approach: combination of site-directed-mutagenesis-based saturation binding assay and molecular modeling based on the crystallographic data of bovine rhodopsin.[22] The site-directed-mutagenesis-based saturation binding assay alone can give certain insights as to which residues of the receptor are implicated in the binding with the inhibitor. However, it does not indicate which specific atoms of the residue are involved. Homology modeling and docking give insights to interactions between atoms, but these methods produce multiple possible solutions, and it is difficult to differentiate between distinct interactions that are within a small energy range. Combining these complementary methods of site-directed mutagenesis and computational protein structure determination has made it possible to conduct robust structural analyses.[22] However, certain validation of the model is crucial. Thus, in the present study, we chose five amino acid residues of CCR5 that were judged to be critical for APL binding based on our previous analysis, and additional mutagenesis studies were carried out. When an amino acid substitution (P84H, C101A, F109A, T195P, or T195S) was introduced into $CCR5_{WT}$ and saturation binding assay was performed using [$^3$H]APL, all $K_d$ values proved to be >100 nM, while the $K_d$ value of [$^3$H]APL with wild-type CCR5 was 3.6 nM. This corroborated the notion that we previously made[22]—that the alternate approach using saturation binding assay, combined with our computational protein structure determination, can provide reasonably robust structural insights.

In the present study, we attempted to obtain a refined structural CCR5 model through molecular dynamics computation. In an unbound CCR5, we identified key interactions between residues located in different transmembranes, and between transmembrane and ECL2 amino acid residues. Amino acids involved in such intramolecular interactions included Y37, H175, Y108, Y251, E283, and S180. The intramolecular hydrogen bond interactions observed among different transmembrane regions, and between transmembrane and ECL2 loop presumably stabilize the unbound conformation of CCR5 (Fig. 3). In order to determine the structures of AK317, and AK530 complexed to CCR5, we utilized a novel algorithm to incorporate receptor flexibility and induced-fit effects.[38] The optimized AK317–CCR5 and AK530–CCR5 complex structures indica-

ted a rotation of Y108(TM3) away from both Y251 (TM6) and E283(TM7) to make room for the inhibitor within the transmembrane helices. As a result of inhibitor binding, the hydrogen bond between Y108 and E283 and that between E283 and S180 seen in the unliganded CCR5 were disrupted, and these residues formed hydrogen bond or tight van der Waals interactions with the inhibitors instead (Figs. 5–7). The disruption of interhelix residue interactions may cause movement of the transmembrane helices and changes in the conformation of ECL2. A similar mechanism, involving disruption of interhelix hydrogen bond interactions, is thought to be responsible for changes in loop conformation in rhodopsin[27,29] and in the activation of $\beta_2$-adrenergic receptor.[34] Note that Y37(TM1) is involved in a hydrogen bond interaction with ECL2 via H175. We have observed that Y37 interacts with SCH-C and TAK-779.[22] These arrangements of hydrogen bond interactions between transmembrane helices and ECL2 should also provide an explanation of the reason that these inhibitors exert potent antiviral activity against HIV-1. Thus, the disruption of hydrogen bond interactions between transmembrane helices, and between transmembrane helices and ECL2, should be a mechanism of allosteric inhibition observed by the binding of CCR5 inhibitors to a binding domain residing mostly within the transmembrane residues.

We also examined the interplays of ECL2 and selected amino acid residues that consist of the largest hydrophobic cavity within CCR5, which accommodate small-molecule CCR5 inhibitors. Our previously published data[22] and data by others[19,23] showed that two CCR5 inhibitors (SCH-C and TAK-779) have no direct interactions with amino acid residues in the extracellular domain, including ECL2. However, all the three SDP-based CCR5 inhibitors that we examined (AK530, AK317, and APL) had substantial interactions with amino acids in ECL2, in particular with C178, which is located in the antiparallel β-hairpin structural motif of ECL2, and with K191, which is located at the interface of ECL2 and TM5 (Figs. 4–6). The C178A substitution virtually abrogated the binding of the three inhibitors to CCR5. C178 is presumed to form a disulfide bond with C101 of TM3 and seems to be critical for the conformation of ECL2. The disruption of the disulfide bond with C178A mutation may result in decreased binding of the three SDP-based inhibitors. Our previous observation[22] and the report from others[19,23] that the same C178A substitution did not affect the CCR5 binding of two other CCR5 inhibitors, SCH-C and TAK-779, suggest that C178 plays a unique but critical role in the binding of AK530, AK317, and APL. In the present study, K191A substitution also virtually nullified the CCR5 binding of AK317 and APL (Table 2), although it did not significantly affect the binding of AK530 probably due to the absence of hydrogen bonding between AK530 and K191 (Fig. 5). Taken together, these data suggest that, unlike the cases of SCH-C and TAK-779, at least a part of the hydrophobic cavity where AK530, AK317, and APL are lodged within CCR5 involves ECL2. The disruption of ECL2's β-sheet structure by the removal of disulfide bond through C101A and C178A substitutions virtually nullified both the binding of all three CCR5 inhibitors and the HIV-1-gp120-elicited fusion. This strongly suggests that ECL2 plays a crucial role not only in the binding of the three CCR5 inhibitors but also in the interaction of HIV-1 envelope glycoproteins with CCR5. The data also suggest that at least two amino acids in ECL2, C178 and K191, can be potential targets for the design of CCR5 inhibitors.

Several studies have shown that the resistance against a CCR5 inhibitor emerged without the change in coreceptor usage.[39–44] Resistant R5-HIV-1 variants were reportedly obtained by passage 22 for AD101,[40] passage 43 for TAK-652,[41] passage 20 for VVC,[43] and passages 12–18 for MVC.[42] However, we have failed in selecting R5-HIV-1 variants resistant to APL even after 60 passages *in vitro* (over ~1.5 years) (Nakata *et al.*, unpublished data), although the possibility of the emergence of HIV-1 variants resistant to APL cannot be ruled out in other settings.[45] Pugach *et al.* demonstrated that one of the mechanisms by which HIV-1 becomes resistant to CCR5 inhibitors such as VVC is by "noncompetitive resistance"—a process in which a resistant virus continues to enter target cells regardless of the concentration of the inhibitor once HIV-1 has acquired the ability to use the inhibitor-bound CCR5 for entry.[44] Of note, Westby *et al.* reported that a virus resistant to MVC retained susceptibility to APL, suggesting that the virus can use MVC-bound CCR5 for entry, but cannot use APL-bound CCR5.[42] Thus, APL is likely to have such a profile that does not allow or delay HIV-1 acquisition of the ability to utilize the "APL-bound" CCR5 for its cellular entry. This potentially favorable property of APL may be related to the direct interactions of APL with amino acids in ECL2, producing "substantially distorted" ECL2 with which HIV-1 gp120 cannot get engaged for its cellular entry, while certain unique allosteric changes in ECL2 conformation following the binding of APL might also explain the substantial delay or lack of the emergence of APL-resistant HIV-1.

The present data, taken together, demonstrate that structural modeling analysis, coupled with CCR5-binding affinity data, should help understand the structural/molecular mechanism of the inhibition of HIV-1 infection by CCR5 inhibitors. The data should not only help delineate the structural dynamics of CCR5 following ligand binding but also aid in the design of therapeutic inhibitors. The data, in particular, demonstrate that by studying the properties of unbound and inhibitor-bound CCR5, transmembrane residues such as Y108, Y251, and E283 are important for gp120 fusion, HIV infectivity,[22] and inhibitor binding. The loss of hydrogen bond interactions among these key transmembrane residues and the interactions between E283 and S180, which are essential for the formation and maintenance of the binding pocket for CCR5 inhibitors, might be responsible for changes in ECL2 conformation, providing insights into the mechanism of gp120 inhibition.

## Materials and Methods

### Reagents

Three SDP derivatives, APL,[14,46] AK530, and AK317, are discussed in the present report. The methods for the synthesis and physicochemical profiles of AK530 and AK317 will be described elsewhere. Tritiation of these three CCR5 inhibitors was conducted as previously reported.[14] The structures of these three CCR5 inhibitors are illustrated in Fig. 1.

### Cells, viruses, and anti-HIV-1 assay

CHO cells expressing wild-type CCR5 ($CCR5_{WT}$-CHO cells) or mutant CCR5 ($CCR5_{MT}$-CHO cells)[22] were maintained in Ham's F-12 medium (Invitrogen, Carlsbad, CA), supplemented with 10% fetal calf serum (FCS; HyClone, Logan, UT) in the presence of 100 μg/ml zeomycin (Invitrogen). The MAGI cell line[47] was provided by the National Institutes of Health (NIH) AIDS Research and Reference Reagent Program and cultured in Dulbecco's modified Eagle's medium (DMEM) supplemented with 10% FCS, 200 μg/ml G418, and 100 μg/ml hygromycin B. MAGI-CCR5 cells[48] were maintained in DMEM supplemented with 10% FCS, 200 μg/ml G418, 100 μg/ml hygromycin B, and 100 μg/ml zeomycin. 293T cells were cultured in DMEM with 10% FCS. PBM cells were isolated from buffy coats of HIV-1-seronegative individuals and activated with 10 μg/ml PHA prior to use, as previously described.[8] Two wild-type R5-HIV-1 strains were employed for drug susceptibility assays: $HIV\text{-}1_{Ba\text{-}L}$[49] and $HIV\text{-}1_{JRFL}$.[50] Antiviral assays using PHA-PBM (p24 assay) and MAGI assay using MAGI-CCR5 cells were also conducted as previously reported.[8]

### Fluorescence-activated cell sorter analysis and mAb displacement assay

$CCR5_{WT}$-CHO cells ($2 \times 10^5$) were exposed to differing concentrations (1 nM–1 μM) of a CCR5 inhibitor for 30 min, followed by the addition of a fluorescein-isothiocyanate-conjugated anti-CCR5 mAb, 2D7 (BD PharMingen, San Diego, CA), 45523, 45531, or 45549 (R&D Systems, Minneapolis, MN), and further incubated for 30 min at 4 °C. Cells were washed and analyzed on an flow cytometer (FACSCalibur; BD Biosciences, San Jose, CA). Each fluorescent activity in the presence of a drug was compared to that obtained in the absence of inhibitors and shown as percent control.

### Saturation binding assay

A panel of mutant CCR5-expressing CHO cells[22] was used for saturation binding assays. The CHO cell lines expressing mutant CCR5 P84H ($CCR5_{P84H}$-CHO cells), C101A, L104D, F109A, T195A, T195P, T195S, and W248A were newly generated and used. The saturation binding assay using tritiated CCR5 inhibitors ([$^3$H]APL, [$^3$H]AK530, and [$^3$H]AK317) and wild-type or mutant CCR5-expressing CHO cells was conducted as previously described.[14] In brief, wild-type or mutant $CCR5^+$ CHO cells ($1.5 \times 10^5$ cells/well) were plated onto 48-well flat-bottomed culture plates, incubated for 24 h, exposed to various concentrations of each [$^3$H]CCR5 inhibitor, washed thoroughly, and lysed with 0.5 ml of 1 N NaOH, and radioactivity in the lysates was measured. The $K_d$ (dissociation) values of CCR5 inhibitors and the maximal binding values ($B_{max}$ = number of CCR5 per cell) were calculated based on their specific radioactivity using GRAPHPAD PRISM software (Intuitive Software for Science, San Diego, CA).

### CCR5 homology model

A homology model of CCR5 was built as follows. The sequence of CCR5 (352 amino acids) was aligned against the sequence of bovine rhodopsin (348 amino acids). The recently determined crystal structure of bovine rhodopsin by Okada *et al.* was used as the template structure [Protein Data Bank (PDB) accession ID 1U19].[27] The alignment was manually adjusted to ensure that the conserved GPCR residues were aligned as follows: in TM1, N55 of bovine rhodopsin was aligned to N48 of CCR5; in TM2, D83 was aligned to D76; in TM3, E134-R135-Y136 was aligned to D125-R126-Y127; in TM4, W161 was aligned to W153; in TM5, P215 was aligned to P206; in TM6, W265-x266-P267-Y268 was aligned to W248-x249-P250-Y251; in TM7, P303 was aligned to P294; in H8, F313 was aligned to F304. Secondary structure prediction assigned the length of each helix, β-sheet, and loop segment. After building the transmembrane helices, the loops connecting the different transmembrane domains were built using the ultraextended sampling protocol in Prime (Prime, version 1.6, 2007; Schrödinger, LLC, New York, NY), which does a more exhaustive sampling of the loop conformations.[51] The side chains were predicted using the rotamer library of Xiang and Honig.[52] The structure was minimized in implicit water with the OPLS2005 force field,[53] as implemented in MacroModel (MacroModel 9.1, 2005; Schrödinger, LLC).

All atom molecular dynamics simulations, without using any nonbonded cutoff distances, were carried out on CCR5. A constant temperature of 300 K and SHAKE constraints for hydrogen bonds were used. The GB/SA continuum solvation model, with water as the solvent, was used.[54] Using a time step of 1 fs, the structures were equilibrated for 100 ps. The simulation was carried out for 4800 ps on a Linux cluster, and structures were monitored at 50-ps intervals.

### Structural modeling of the interactions of CCR5 inhibitors with CCR5

After building the initial model of CCR5, the CCR5–inhibitor complex structures were further defined with an iterative optimization of CCR5 and ligand structures in the presence of each other, using software tools from Schrödinger, LLC, as described below. The conformational flexibilities of both CCR5 and CCR5 inhibitors were taken into account. The molecular structures of AK530, AK317, and APL were obtained by minimization using the MMFF94 force field, as implemented in MacroModel. For each minimized inhibitor configuration, a set of low-energy structures was generated by performing a Monte Carlo sampling of their conformations. Thus, obtained structures were used as starting structures for docking calculations where their conformations were further refined.

The protonation states of CCR5 residues were assigned, and residues more than 20 Å from the active site were neutralized. We initially failed to obtain energetically favorable inhibitor–CCR5 complex structures by using a *rigid* CCR5 structure because of the unfavorable steric interaction of the side chains of the active site residues with the inhibitors. In an attempt to place an inhibitor within CCR5, after analysis of the steric clashes, the active site

was artificially enlarged by mutating Y108, C178, E283, and M287 to Ala. The van der Waals radii of inhibitor atoms were scaled by a factor of 0.70 to reduce steric clashes and docked into CCR5. After obtaining an initial "guess" set of CCR5–inhibitor complexes, residues 108, 178, 283, and 287 were mutated back from Ala to their original states. CCR5 atoms within 15 Å of an initially placed inhibitor were subsequently refined. It was achieved by using the rotamer library of Xiang and Honig and by optimizing each side chain one at a time, holding all other side chains fixed.[52] After convergence, all side chains were simultaneously energy-minimized to remove any remaining clashes. The inhibitors were docked again and scored to estimate their relative affinity. The extraprecision mode of Glide,[55,56] which penalized unfavorable and unphysical interactions, was used. The docked complexes with higher scores were visually examined along with the mutational data to select the best possible CCR5–inhibitor complex.

Visualization, structural refinement, and docking were performed using Maestro 7.5, MacroModel 9.1, Prime 1.6, Glide 4.5, and IFD script[38] from Schrödinger, LLC (2007). Computations were carried out on a multiprocessor SGI Origin 3400 computer platform and on a Beowulf-type Linux cluster.

### HIV-1-gp120-elicited cell–cell fusion assay

The entire human *CCR5* gene, including a stop codon, was amplified using pZeoSV-*CCR5*[48] as template. The polymerase chain reaction product was ligated into pcDNA6.2/cLumio-DEST vector (Invitrogen), cloned in accordance with the manufacturer's recommendation, and termed pcDNA6.2-CCR5$_{WT}$ (a CCR5 expression vector). A variety of plasmids carrying a mutant *CCR5*-encoding gene (pcDNA6.2-*CCR5*$_{MT}$) were subsequently generated by employing the site-directed mutagenesis technique. An HIV-1 *tat* expression vector (pcDNA6.2-HIV-*tat*) was also generated using the same method. For the generation of HIV-1-gp120-overexpressing 293T cells, an HIV envelope expression vector, pCXN-J*Renv*,[48] was employed. A reporter (luciferase) gene containing plasmid pLTR-*Luc*E[57] was provided by the NIH AIDS Research and Reference Reagent Program. The envelope expression vector and tat expression vector (0.5 μg each) were cotransfected into 293T cells ($2\times10^5$; 3 ml in six-well microculture plates) using Lipofectamine 2000 (Invitrogen), while the CCR5$_{WT}$ or mutant CCR5 expression vector and pLTR-*Luc*E (0.5 μg each) were cotransfected into MAGI cells ($2\times10^5$; 3 ml in six-well microculture plates). On the next day, both the cotransfected cells were harvested and mixed in a well of 96-well plates ($2\times10^4$ cells each). The cotransfected cells were incubated further for 6 h, the luciferase activity in each well was detected using Bright-Glo Luciferase Assay System (Promega, Madison, WI), and its luminescence level was measured using Veritas Microplate Luminometer (Turner BioSystmes, Sunnyvale, CA). Nonspecific luciferase activity was determined with the luminescence level in the well containing control tat$^+$,env$^-$ 293T cells and Luc$^+$,CCR5$^+$ MAGI cells, and the value of the nonspecific luminescence level was subtracted from each experimental luminescence level.

### Protein Model DataBase accession code

The coordinates for the models of ligand-free CCR5, CCR5–AK317, and CCR5–AK530 complexes with accession codes PM0075224, PM0075223, and PM0075221, respectively, have been deposited in the Protein Model DataBase†.

## Acknowledgements

The authors thank David A. Davis and Yasuhiro Koh for critical reading of the manuscript. This work was supported, in part, by the Intramural Research Program of the Center for Cancer Research, National Cancer Institute, NIH, and in part by a Grant for the Promotion of AIDS Research from the Ministry of Health, Welfare, and Labor of Japan, and the Grant to the Cooperative Research Project on Clinical and Epidemiological Studies of Emerging and Reemerging Infectious Diseases (Renkei Jigyo: No. 78, Kumamoto University) of Monbu-Kagakusho (H. M.). We also thank the Center for Information Technology, NIH, for providing computational resources on the NIH Beowulf Linux cluster, and Susan Chacko and David Hoover for help with batch job configuration on the cluster.

## References

1. Raport, C. J., Gosling, J., Schweickart, V. L., Gray, P. W. & Charo, I. F. (1996). Molecular cloning and functional characterization of a novel human CC chemokine receptor (CCR5) for RANTES, MIP-1beta, and MIP-1alpha. *J. Biol. Chem.* **271**, 17161–17166.
2. Alkhatib, G., Combadiere, C., Broder, C. C., Feng, Y., Kennedy, P. E., Murphy, P. M. & Berger, E. A. (1996). CC CKR5: a RANTES, MIP-1alpha, MIP-1beta receptor as a fusion cofactor for macrophage-tropic HIV-1. *Science*, **272**, 1955–1958.
3. Wu, L., Gerard, N. P., Wyatt, R., Choe, H., Parolin, C., Ruffing, N. *et al.* (1996). CD4-induced interaction of primary HIV-1 gp120 glycoproteins with the chemokine receptor CCR-5. *Nature*, **384**, 179–183.
4. Trkola, A., Dragic, T., Arthos, J., Binley, J. M., Olson, W. C., Allaway, G. P. *et al.* (1996). CD4-dependent, antibody-sensitive interactions between HIV-1 and its co-receptor CCR-5. *Nature*, **384**, 184–187.
5. Deng, H., Liu, R., Ellmeier, W., Choe, S., Unutmaz, D., Burkhart, M. *et al.* (1996). Identification of a major co-receptor for primary isolates of HIV-1. *Nature*, **381**, 661–666.
6. Kilby, J. M. & Eron, J. J. (2003). Novel therapies based on mechanisms of HIV-1 cell entry. *N. Engl. J. Med.* **348**, 2228–2238.
7. Baba, M., Nishimura, O., Kanzaki, N., Okamoto, M., Sawada, H., Iizawa, Y. *et al.* (1999). A small-molecule, nonpeptide CCR5 antagonist with highly potent and selective anti-HIV-1 activity. *Proc. Natl Acad. Sci. USA*, **96**, 5698–5703.
8. Maeda, K., Yoshimura, K., Shibayama, S., Habashita, H., Tada, H., Sagawa, K. *et al.* (2001). Novel low molecular weight spirodiketopiperazine derivatives potently inhibit R5 HIV-1 infection through their antagonistic effects on CCR5. *J. Biol. Chem.* **276**, 35194–35200.

† http://mi.caspur.it/PMDB

9. Watson, C., Jenkinson, S., Kazmierski, W. & Kenakin, T. (2005). The CCR5 receptor-based mechanism of action of 873140, a potent allosteric noncompetitive HIV entry inhibitor. *Mol. Pharmacol.* **67**, 1268–1282.
10. Tagat, J. R., McCombie, S. W., Nazareno, D., Labroli, M. A., Xiao, Y., Steensma, R. W. *et al.* (2004). Piperazine-based CCR5 antagonists as HIV-1 inhibitors: IV. Discovery of 1-[(4,6-dimethyl-5-pyrimidinyl)carbonyl]-4-[4-[2-methoxy-1(*R*)-4-(trifluoromethyl)phenyl] ethyl-3(*S*)-methyl-1-piperaz inyl]-4-methylpiperidine (Sch-417690/Sch-D), a potent, highly selective, and orally bioavailable CCR5 antagonist. *J. Med. Chem.* **47**, 2405–2408.
11. Dorr, P., Westby, M., Dobbs, S., Griffin, P., Irvine, B., Macartney, M. *et al.* (2005). Maraviroc (UK-427,857), a potent, orally bioavailable, and selective small-molecule inhibitor of chemokine receptor CCR5 with broad-spectrum anti-human immunodeficiency virus type 1 activity. *Antimicrob. Agents Chemother.* **49**, 4721–4732.
12. Seto, M., Aikawa, K., Miyamoto, N., Aramaki, Y., Kanzaki, N., Takashima, K. *et al.* (2006). Highly potent and orally active CCR5 antagonists as anti-HIV-1 agents: synthesis and biological activities of 1-benzazocine derivatives containing a sulfoxide moiety. *J. Med. Chem.* **49**, 2037–2048.
13. Imamura, S., Ichikawa, T., Nishikawa, Y., Kanzaki, N., Takashima, K., Niwa, S. *et al.* (2006). Discovery of a piperidine-4-carboxamide CCR5 antagonist (TAK-220) with highly potent anti-HIV-1 activity. *J. Med. Chem.* **49**, 2784–2793.
14. Maeda, K., Nakata, H., Koh, Y., Miyakawa, T., Ogata, H., Takaoka, Y. *et al.* (2004). Spirodiketopiperazine-based CCR5 inhibitor which preserves CC-chemokine/CCR5 interactions and exerts potent activity against R5 human immunodeficiency virus type 1 *in vitro*. *J. Virol.* **78**, 8654–8662.
15. Fatkenheuer, G., Pozniak, A. L., Johnson, M. A., Plettenberg, A., Staszewski, S., Hoepelman, A. I. *et al.* (2005). Efficacy of short-term monotherapy with maraviroc, a new CCR5 antagonist, in patients infected with HIV-1. *Nat. Med.* **11**, 1170–1172.
16. Cormier, E. G. & Dragic, T. (2002). The crown and stem of the V3 loop play distinct roles in human immunodeficiency virus type 1 envelope glycoprotein interactions with the CCR5 coreceptor. *J. Virol.* **76**, 8953–8957.
17. Huang, C. C., Tang, M., Zhang, M. Y., Majeed, S., Montabana, E., Stanfield, R. L. *et al.* (2005). Structure of a V3-containing HIV-1 gp120 core. *Science*, **310**, 1025–1028.
18. Kondru, R., Zhang, J., Ji, C., Mirzadegan, T., Rotstein, D., Sankuratri, S. & Dioszegi, M. (2008). Molecular interactions of CCR5 with major classes of small-molecule anti-HIV CCR5 antagonists. *Mol. Pharmacol.* **73**, 789–800.
19. Dragic, T., Trkola, A., Thompson, D. A., Cormier, E. G., Kajumo, F. A., Maxwell, E. *et al.* (2000). A binding pocket for a small molecule inhibitor of HIV-1 entry within the transmembrane helices of CCR5. *Proc. Natl Acad. Sci. USA*, **97**, 5639–5644.
20. Nishikawa, M., Takashima, K., Nishi, T., Furuta, R. A., Kanzaki, N., Yamamoto, Y. & Fujisawa, J. (2005). Analysis of binding sites for the new small-molecule CCR5 antagonist TAK-220 on human CCR5. *Antimicrob. Agents Chemother.* **49**, 4708–4715.
21. Seibert, C., Ying, W., Gavrilov, S., Tsamis, F., Kuhmann, S. E., Palani, A. *et al.* (2006). Interaction of small molecule inhibitors of HIV-1 entry with CCR5. *Virology*, **349**, 41–54.
22. Maeda, K., Das, D., Ogata-Aoki, H., Nakata, H., Miyakawa, T., Tojo, Y. *et al.* (2006). Structural and molecular interactions of CCR5 inhibitors with CCR5. *J. Biol. Chem.* **281**, 12688–12698.
23. Tsamis, F., Gavrilov, S., Kajumo, F., Seibert, C., Kuhmann, S., Ketas, T. *et al.* (2003). Analysis of the mechanism by which the small-molecule CCR5 antagonists SCH-351125 and SCH-350581 inhibit human immunodeficiency virus type 1 entry. *J. Virol.* **77**, 5201–5208.
24. Nakata, H., Maeda, K., Miyakawa, T., Shibayama, S., Matsuo, M., Takaoka, Y. *et al.* (2005). Potent anti-R5 human immunodeficiency virus type 1 effects of a CCR5 antagonist, AK602/ONO4128/GW873140, in a novel human peripheral blood mononuclear cell nonobese diabetic-SCID, interleukin-2 receptor gamma-chain-knocked-out AIDS mouse model. *J. Virol.* **79**, 2087–2096.
25. Wu, L., LaRosa, G., Kassam, N., Gordon, C. J., Heath, H., Ruffing, N. *et al.* (1997). Interaction of chemokine receptor CCR5 with its ligands: multiple domains for HIV-1 gp120 binding and a single domain for chemokine binding. *J. Exp. Med.* **186**, 1373–1381.
26. Samson, M., LaRosa, G., Libert, F., Paindavoine, P., Detheux, M., Vassart, G. & Parmentier, M. (1997). The second extracellular loop of CCR5 is the major determinant of ligand specificity. *J. Biol. Chem.* **272**, 24934–24941.
27. Okada, T., Sugihara, M., Bondar, A. N., Elstner, M., Entel, P. & Buss, V. (2004). The retinal conformation and its environment in rhodopsin in light of a new 2.2 A crystal structure. *J. Mol. Biol.* **342**, 571–583.
28. Gether, U. & Kobilka, B. K. (1998). G protein-coupled receptors: II. Mechanism of agonist activation. *J. Biol. Chem.* **273**, 17979–17982.
29. Farrens, D. L., Altenbach, C., Yang, K., Hubbell, W. L. & Khorana, H. G. (1996). Requirement of rigid-body motion of transmembrane helices for light activation of rhodopsin. *Science*, **274**, 768–770.
30. Okada, T., Fujiyoshi, Y., Silow, M., Navarro, J., Landau, E. M. & Shichida, Y. (2002). Functional role of internal water molecules in rhodopsin revealed by X-ray crystallography. *Proc. Natl Acad. Sci. USA*, **99**, 5982–5987.
31. Siciliano, S. J., Kuhmann, S. E., Weng, Y., Madani, N., Springer, M. S., Lineberger, J. E. *et al.* (1999). A critical site in the core of the CCR5 chemokine receptor required for binding and infectivity of human immunodeficiency virus type 1. *J. Biol. Chem.* **274**, 1905–1913.
32. Palczewski, K., Kumasaka, T., Hori, T., Behnke, C. A., Motoshima, H., Fox, B. A. *et al.* (2000). Crystal structure of rhodopsin: a G protein-coupled receptor. *Science*, **289**, 739–745.
33. Rosenkilde, M. M. & Schwartz, T. W. (2006). GluVII:06—a highly conserved and selective anchor point for non-peptide ligands in chemokine receptors. *Curr. Top. Med. Chem.* **6**, 1319–1333.
34. Ballesteros, J. A., Jensen, A. D., Liapakis, G., Rasmussen, S. G., Shi, L., Gether, U. & Javitch, J. A. (2001). Activation of the beta 2-adrenergic receptor involves disruption of an ionic lock between the cytoplasmic ends of transmembrane segments 3 and 6. *J. Biol. Chem.* **276**, 29171–29177.
35. Olson, W. C., Rabut, G. E., Nagashima, K. A., Tran, D. N., Anselma, D. J., Monard, S. P. *et al.* (1999). Differential inhibition of human immunodeficiency virus type 1 fusion, gp120 binding, and CC-chemokine activity by monoclonal antibodies to CCR5. *J. Virol.* **73**, 4145–4155.
36. Lee, B., Sharron, M., Blanpain, C., Doranz, B. J., Vakili, J., Setoh, P. *et al.* (1999). Epitope mapping of CCR5 reveals multiple conformational states and distinct but overlapping structures involved in chemokine and coreceptor function. *J. Biol. Chem.* **274**, 9617–9626.

37. Rasmussen, S. G., Choi, H. J., Rosenbaum, D. M., Kobilka, T. S., Thian, F. S., Edwards, P. C. *et al.* (2007). Crystal structure of the human beta$_2$ adrenergic G-protein-coupled receptor. *Nature*, **450**, 383–387.
38. Sherman, W., Day, T., Jacobson, M. P., Friesner, R. A. & Farid, R. (2006). Novel procedure for modeling ligand/receptor induced fit effects. *J. Med. Chem.* **49**, 534–553.
39. Kuhmann, S. E., Pugach, P., Kunstman, K. J., Taylor, J., Stanfield, R. L., Snyder, A. *et al.* (2004). Genetic and phenotypic analyses of human immunodeficiency virus type 1 escape from a small-molecule CCR5 inhibitor. *J. Virol.* **78**, 2790–2807.
40. Trkola, A., Kuhmann, S. E., Strizki, J. M., Maxwell, E., Ketas, T., Morgan, T. *et al.* (2002). HIV-1 escape from a small molecule, CCR5-specific entry inhibitor does not involve CXCR4 use. *Proc. Natl Acad. Sci. USA*, **99**, 395–400.
41. Baba, M., Miyake, H., Wang, X., Okamoto, M. & Takashima, K. (2007). Isolation and characterization of human immunodeficiency virus type 1 resistant to the small-molecule CCR5 antagonist TAK-652. *Antimicrob. Agents Chemother.* **51**, 707–715.
42. Westby, M., Smith-Burchnell, C., Mori, J., Lewis, M., Mosley, M., Stockdale, M. *et al.* (2007). Reduced maximal inhibition in phenotypic susceptibility assays indicates that viral strains resistant to the CCR5 antagonist maraviroc utilize inhibitor-bound receptor for entry. *J. Virol.* **81**, 2359–2371.
43. Marozsan, A. J., Kuhmann, S. E., Morgan, T., Herrera, C., Rivera-Troche, E., Xu, S. *et al.* (2005). Generation and properties of a human immunodeficiency virus type 1 isolate resistant to the small molecule CCR5 inhibitor, SCH-417690 (SCH-D). *Virology*, **338**, 182–199.
44. Pugach, P., Marozsan, A. J., Ketas, T. J., Landes, E. L., Moore, J. P. & Kuhmann, S. E. (2007). HIV-1 clones resistant to a small molecule CCR5 inhibitor use the inhibitor-bound form of CCR5 for entry. *Virology*, **361**, 212–228.
45. LaBranche, C., Kitrinos, K., Howell, R., McDanal, C., Harris, S., Jeffrey, J. & Demarest, J. (2005). Targeting HIV Entry, 1st International Workshop, Bethesda, MD, December 2–3, Abstract 9.
46. Nishizawa, R., Nishiyama, T., Hisaichi, K., Matsunaga, N., Minamoto, C., Habashita, H. *et al.* (2007). Spirodiketopiperazine-based CCR5 antagonists: lead optimization from biologically active metabolite. *Bioorg. Med. Chem. Lett.* **17**, 727–731.
47. Kimpton, J. & Emerman, M. (1992). Detection of replication-competent and pseudotyped human immunodeficiency virus with a sensitive cell line on the basis of activation of an integrated beta-galactosidase gene. *J. Virol.* **66**, 2232–2239.
48. Maeda, Y., Foda, M., Matsushita, S. & Harada, S. (2000). Involvement of both the V2 and V3 regions of the CCR5-tropic human immunodeficiency virus type 1 envelope in reduced sensitivity to macrophage inflammatory protein 1alpha. *J. Virol.* **74**, 1787–1793.
49. Gartner, S., Markovits, P., Markovitz, D. M., Kaplan, M. H., Gallo, R. C. & Popovic, M. (1986). The role of mononuclear phagocytes in HTLV-III/LAV infection. *Science*, **233**, 215–219.
50. Koyanagi, Y., O'Brien, W. A., Zhao, J. Q., Golde, D. W., Gasson, J. C. & Chen, I. S. (1988). Cytokines alter production of HIV-1 from primary mononuclear phagocytes. *Science*, **241**, 1673–1675.
51. Jacobson, M. P., Pincus, D. L., Rapp, C. S., Day, T. J., Honig, B., Shaw, D. E. & Friesner, R. A. (2004). A hierarchical approach to all-atom protein loop prediction. *Proteins*, **55**, 351–367.
52. Xiang, Z. & Honig, B. (2001). Extending the accuracy limits of prediction for side-chain conformations. *J. Mol. Biol.* **311**, 421–430.
53. Kaminski, G. A., Friesner, R. A., Tirado-Rives, J. & Jorgensen, W. J. (2001). Evaluation and reparameterization of the OPLS-AA force field for proteins via comparison with accurate quantum chemical calculations on peptides. *J. Phys. Chem. B*, **105**, 6474–6487.
54. Still, W. C., Tempczyk, A., Hawley, R. C. & Hendrickson, T. (1990). Semianalytical treatment of solvation for molecular mechanics and dynamics. *J. Am. Chem. Soc.* **112**, 6127–6129.
55. Friesner, R. A., Banks, J. L., Murphy, R. B., Halgren, T. A., Klicic, J. J., Mainz, D. T. *et al.* (2004). Glide: a new approach for rapid, accurate docking and scoring: 1. Method and assessment of docking accuracy. *J. Med. Chem.* **47**, 1739–1749.
56. Friesner, R. A., Murphy, R. B., Repasky, M. P., Frye, L. L., Greenwood, J. R., Halgren, T. A. *et al.* (2006). Extra precision Glide: docking and scoring incorporating a model of hydrophobic enclosure for protein–ligand complexes. *J. Med. Chem.* **49**, 6177–6196.
57. Jeeninga, R. E., Hoogenkamp, M., Armand-Ugon, M., de Baar, M., Verhoef, K. & Berkhout, B. (2000). Functional differences between the long terminal repeat transcriptional promoters of human immunodeficiency virus type 1 subtypes A through G. *J. Virol.* **74**, 3740–3751.

The International Journal of Biochemistry & Cell Biology 40 (2008) 2410–2420

Contents lists available at ScienceDirect

The International Journal of Biochemistry & Cell Biology

journal homepage: www.elsevier.com/locate/biocel

# 2′-Deoxy-4′-C-ethynyl-2-halo-adenosines active against drug-resistant human immunodeficiency virus type 1 variants

Atsushi Kawamoto[a], Eiichi Kodama[a,*], Stefan G. Sarafianos[b], Yasuko Sakagami[a], Satoru Kohgo[c], Kenji Kitano[c], Noriyuki Ashida[c], Yuko Iwai[c], Hiroyuki Hayakawa[c], Hirotomo Nakata[d,e], Hiroaki Mitsuya[d,e], Eddy Arnold[f], Masao Matsuoka[a]

[a] *Laboratory of Virus Immunology, Institute for Virus Research, Kyoto University, 53 Kawaramachi, Shogoin, Sakyo-ku, Kyoto 606-8507, Japan*
[b] *Department of Molecular Microbiology and Immunology, University of Missouri-Columbia, School of Medicine and Christopher S. Bond Life Sciences Center, Columbia, MO 65211, USA*
[c] *Biochemicals Division, Yamasa Corporation, Chiba 288-0056, Japan*
[d] *Department of Hematology and Infectious Diseases, Kumamoto University School of Medicine, Kumamoto 860-8556, Japan*
[e] *Experimental Retrovirology Section, HIV and AIDS Malignancy Branch, National Cancer Institute, Bethesda, MD 20892, USA*
[f] *Center for Advanced Biotechnology and Medicine and Department of Chemistry and Chemical Biology, Rutgers University, Piscataway, NJ 08854, USA*

ARTICLE INFO

*Article history:*
Received 3 December 2007
Received in revised form 14 March 2008
Accepted 2 April 2008
Available online 11 April 2008

*Keywords:*
Human immunodeficiency virus
Reverse transcriptase inhibitor
Resistance

ABSTRACT

One of the formidable challenges in therapy of infections by human immunodeficiency virus (HIV) is the emergence of drug-resistant variants that attenuate the efficacy of highly active antiretroviral therapy (HAART). We have recently introduced 4′-ethynyl-nucleoside analogs as nucleoside reverse transcriptase inhibitors (NRTIs) that could be developed as therapeutics for treatment of HIV infections. In this study, we present 2′-deoxy-4′-C-ethynyl-2-fluoroadenosine (EFdA), a second generation 4′-ethynyl inhibitor that exerted highly potent activity against wild-type HIV-1 ($EC_{50} \sim 0.07$ nM). EFdA retains potency toward many HIV-1 resistant strains, including the multi-drug resistant clone HIV-$1_{A62V/V75I/F77L/F116Y/Q151M}$. The selectivity index of EFdA (cytotoxicity/inhibitory activity) is more favorable than all approved NRTIs used in HIV therapy. Furthermore, EFdA efficiently inhibited clinical isolates from patients heavily treated with multiple anti-HIV-1 drugs. EFdA appears to be primarily phosphorylated by the cellular 2′-deoxycytidine kinase (dCK) because: (a) the antiviral activity of EFdA was reduced by the addition of dC, which competes nucleosides phosphorylated by the dCK pathway, (b) the antiviral activity of EFdA was significantly reduced in dCK-deficient HT-1080/Ara-$C^r$ cells, but restored after dCK transduction. Further, unlike other dA analogs, EFdA is completely resistant to degradation by adenosine deaminase. Moderate decrease in susceptibility to EFdA is conferred by a combination of three RT mutations (I142V, T165R, and M184V) that result in a significant decrease of viral fitness. Molecular modeling analysis suggests that the M184V/I substitutions may reduce anti-HIV activity of EFdA through steric hindrance between its 4′-ethynyl moiety and the V/I184 β-branched side chains. The present data suggest that EFdA, is a promising candidate for developing as a therapeutic agent for the treatment of individuals harboring multi-drug resistant HIV variants.



## 1. Introduction

Highly active antiretroviral therapies (HAART), combining two or more reverse transcriptase inhibitors (RTIs) and/or protease inhibitors, have been successful in sig-

* Corresponding author. Tel.: +81 75 751 3986; fax: +81 75 751 3986.
*E-mail address:* ekodama@virus.kyoto-u.ac.jp (E. Kodama).

1357-2725/$ – see front matter © 2008 Elsevier Ltd. All rights reserved.
doi:10.1016/j.biocel.2008.04.007

nificantly reducing viral loads and bringing about clinical benefits to the treatment of patients infected with human immunodeficiency virus type 1 (HIV-1). Although HAART improves prognosis for HIV-1 infected patients (Palella et al., 1998), drug-resistant viruses emerge during prolonged therapy and some resistant viruses show intra-class cross resistance. Moreover, drug-resistant variants can be transmitted to other individuals as primary infections (Little et al., 2002). Hence, there is a great need for the development of new HIV inhibitors that retain activity against drug-resistant HIV variants.

In this regard, we have focused on the family of nucleoside reverse transcriptase inhibitors (NRTIs) and have previously reported that a series of 2′-deoxy-4′-*C*-ethynyl-nucleosides (EdNs) efficiently suppress ($EC_{50}$s as low as one nanomolar) various NRTI-resistant HIV strains including multi-drug resistant clinical isolates (Kodama et al., 2001). More recently, Haraguchi and others have reported that additional members of EdNs such as 2′,3′-didehydro-3′-deoxy-4′-*C*-ethynyl-thymidine (Ed4T) are also active against wild-type and drug-resistant strains ($EC_{50}$s ranged from 0.16 to 17 μM) and less toxic than d4T (also known as stavudine) *in vitro* (Dutschman et al., 2004; Haraguchi et al., 2003), while 4′-Ed4T is only moderately active against (−)-2′,3′-dideoxy-3′-thiacytidine (3TC or lamivudine)-resistant HIV-$1_{M184V}$ (Nitanda et al., 2005).

To further increase the antiviral activity and reduce the cytotoxicity, we designed and synthesized a second generation of 4′-substituted adenosine analogs with halogen substitutions at their 2-position. We report here that 2′-deoxy-4′-*C*-ethynyl-2-fluoroadenosine (EFdA) exhibits the highest antiviral activity than any other NRTI when assayed against wild-type or NRTI-resistant HIV clones and clinical isolates from patients treated extensively with anti-HIV agents. In addition, unlike other adenosine-based NRTIs, EFdA showed adenosine deaminase (ADA) resistance. We also show that EFdA is primarily activated through phosphorylation by cellular deoxycytidine kinase (dCK). Molecular modeling analysis has been used to rationalize the resistance profile of these analogs toward key NRTI mutations.

## 2. Materials and methods

### 2.1. Compounds

3′-Azido-3′-deoxythymidine (AZT, or zidovudine), 2′,3′-dideoxyinosine (ddI, or didanosine), and 2′,3′-dideoxycytidine (ddC, or zalcitabine) were purchased from Sigma (St. Louis, MO.). 3TC was kindly provided from S. Shigeta (Fukushima Medical University, Fukushima, Japan). A set of EdN analogs were designed and synthesized as described elsewhere (Ohrui, 2006). Their chemical structures are shown in Fig. 1. 2′-Deoxycoformycin (dCF) was synthesized in Yamasa Corporation (Choshi, Japan).

### 2.2. Cells and plasmids

MT-2 and MT-4 cells were grown in an RPMI 1640-based culture medium, and 293T cells were grown in Dulbecco's modified Eagle medium (DMEM); each of these media was

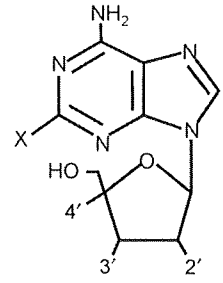


| Base X | Sugar 2′ | Sugar 3′ | 4′ | Compound abbreviation |
|---|---|---|---|---|
| -H | -H | -OH | -C ≡ CH | *E*dA |
| -F | -H | -OH | -C ≡ CH | 2F-*E*dA |
| -F | -H | -H | -C ≡ CH | 2F-*E*ddA |
| -F | C = C | | -C ≡ CH | 2F-*E*d4A |
| -F | -H | -OH | -C ≡ N | 2F-CNdA |
| -Cl | -H | -OH | -C ≡ CH | 2Cl-*E*dA |

**Fig. 1.** Structures of 4′-substituted adenosine analogs. All nucleoside analogs discussed here have substitutions at the 4′-position of the sugar ring.

supplemented with 10% fetal calf serum (FCS), 2 mM L-glutamine, 100 U/ml penicillin, and 50 μg/ml streptomycin. HeLa-CD4-LTR/β-galactosidase (MAGI) cells were propagated in DMEM supplemented with 10% FCS, 0.2 mg/ml of hygromycin B, and 0.2 mg/ml of G418 (Kimpton and Emerman, 1992). HeLa-CD4/CCR5-LTR/β-galactosidase cells were propagated in puromycin (10 μg/ml) containing DMEM with hygromycin and G418. Peripheral blood mononuclear cells (PBMCs) were obtained from healthy HIV-1-seronegative donors by Ficoll-Hypaque gradient centrifugation and stimulated for 3 days with phytohemagglutinin M (PHA; 10 μg/ml; Sigma) and recombinant human interleukin 2 (IL-2; 10 U/ml; Shionogi & Co., Ltd., Osaka, Japan) prior to use. Human fibrosarcoma cell lines, HT-1080 and HT-1080/Ara-$C^r$ were grown in the RPMI-based culture medium (Obata et al., 2001). To express HIV-1 receptors, we constructed a mammalian expression vector pBC-CD4/CXCR4-IH, which encodes CD4, CXCR4, and hygromycin phosphotransferase with two internal ribosome entry sites under control of cytomegalovirus promoter as described (Kajiwara et al., 2006). After the transfection into HT-1080 and HT-1080/Ara-$C^r$, cells were selected by 0.2 mg/ml hygromycin B. For the expression of human deoxycytidine kinase (dCK), pCI-neo (Promega, Madison, WI)-based plasmid, pCI-dCK, was transfected into HT-1080/Ara-$C^r$ and selected with 0.2 mg/ml G418. Established cells were designated HT-1080/Ara-$C^r$/dCK. Puromycin resistance gene under the control of PGK promoter was inserted into pLTR-SEAP (Miyake et al., 2003), which encodes a secreted form of the placental alkaline phosphatase (SEAP) gene under control of the HIV-1 long terminal repeat (LTR) (pLTR-SEAP-$puro^r$). pLTR-SEAP-$puro^r$ was transfected into the three HT-1080 cell lines and selected with 10 μg/ml puromycin.

### 2.3. Viruses and construction of recombinant HIV-1 clones

Two laboratory strains, HIV-$1_{IIIB}$ and HIV-$2_{EHO}$, were used. Multi-drug resistant clinical HIV-1 strains, which had been exposed to over 10 anti-HIV-1 drugs for at least 3 years, were passaged in PHA-stimulated PBMCs (PHA-PBMCs) and stored at −80 °C until further use. Recombinant infectious HIV-1 clones carrying various mutations in the *pol* gene were generated using pNL101 (Jeang et al., 1993). Briefly, desired mutations were introduced into the XmaI–NheI region (759 bp) of pTZNX1, which encoded Gly-15 to Ala-267 of HIV-1 RT (strain BH 10) by a site-directed mutagenesis method (Weiner et al., 1994). The XmaI–NheI fragment was inserted into a pNL101-based plasmid, pNL-RT, generating various molecular clones with the desired mutations. To generate pNL-RT, we first introduced a silent mutation at NheI site of the pNL101, GCTAGC to GCCAGC (underlined; 7251 n.t. from the 5′-LTR) by site-directed mutagenesis. Then, the ApaI–SalI fragment of pNL101 without the NheI site was replaced with that of pSUM9 (Shirasaka et al., 1995), to introduce XmaI and NheI site in the RT coding region. The presence of intended substitutions and the absence of unintended substitutions in the molecular clones were confirmed by sequencing. Each molecular clone (2 μg/ml as DNA) was transfected into 293T cells ($4 \times 10^5$ cells/6-well plate) by FuGENE 6 Transfection Reagent (Roche Diagnostics, Indianapolis, IN). After 24 h, MT-2 cells ($10^6$ cells/well) were added and co-cultured with 293T cells for an additional 24 h. When an extensive cytopathic effect was observed, the cell supernatants were harvested, and the virus was further propagated in MT-4 cells. The culture supernatant was harvested and stored at −80 °C until further use.

### 2.4. Determination of drug susceptibility

The inhibitory effect of test compounds on viral replication for 5 days was evaluated in MT-4 cells by the MTT method as described previously (Kodama et al., 2001). The sensitivity of NRTI-resistant infectious clones to test compounds was determined by the MAGI assay as described (Nameki et al., 2005). The drug susceptibility of HIV-1 clinical isolates was determined on day 7 by a commercially available p24 antigen assay (Kodama et al., 2001). Briefly, PHA-PBMCs ($10^6$ cells/ml) were exposed to each viral preparation at $TCID_{50}$ of 50 and cultivated in 200 μl of culture medium containing various concentration of the drug in 96-well culture plates. All assays were performed in triplicate, and the amounts of p24 antigen produced by the cells into the culture medium were determined. A 2′-deoxynucleoside competition assay was performed by the same way as the MAGI assay. An adenosine deaminase (ADA) inhibitor, dCF, was added for preventing conversion of 2′-deoxyadenosine (dA) to 2′-deoxyinosine (dI) (final concentration 0.4 μM). The effect of dCK expression on activities of test compounds was examined by measurement of SEAP activity in the supernatant. At first, the target cells (HT-1080, HT-1080/Ara-$C^r$, and HT-1080/Ara-$C^r$/dCK) were suspended in 96-well plates ($5.0 \times 10^3$ cells/well). On the following day, the cells were inoculated with HIV-$1_{IIIB}$ (500 MAGI unit/well, giving 500 blue cells in MAGI cells) in the presence of serially diluted compounds. After 48 h incubation, supernatant was collected and SEAP activity in the supernatant was measured using BD Great EscAPe SEAP chemiluminescence detection kit (BD Biosciences Clontech., Palo Alto, CA) and Wallac 1450 MicroBeta Jet Luminometer (PerkinElmer, Wellesley, MA).

### 2.5. The effect of ADA

The effect of ADA on EdA or EFdA was examined by high performance liquid chromatography (HPLC). ADA (0.01 U) derived from bovine intestinal tract was added into 0.5 ml of 0.5 mM EFdA in 50 mM Tris–HCl buffer (pH 7.5), and incubated at 25 °C. Samples were collected each 15 min and analyzed by HPLC.

### 2.6. HIV-1 replication assays

MT-2 cells ($2.5 \times 10^5$ cells/5 ml) were infected with each virus preparation (500 MAGI units) for 4 h. The infected cells were then washed and cultured in a final volume of 5 ml. Culture supernatants (200 μl) were harvested from days 1 to 7 after infection, and the p24 antigen amounts were quantified (Nameki et al., 2005).

For competitive HIV-1 replication assay (CHRA), two titrated infectious clones to be examined were mixed and added to MT-2 cells ($10^5$ cells/3 ml) as described previously (Kosalaraksa et al., 1999; Nameki et al., 2005). To ensure that the two infectious clones being compared were of approximately equal infectivity, a fixed amount (500 MAGI units) of one infectious clone was mixed with three different amounts (250, 500 and 1000 MAGI units) of the other infectious clone. On day 1, one-third of the infected MT-2 cells were harvested, washed twice with phosphate-buffered saline, and the cellular DNA was extracted. The purified DNA was subjected to nested PCR and then direct DNA sequencing. The HIV-1 coculture which best approximated a 50:50 mixture on day 1 was further propagated. Every 4–6 days, the cell-free supernatant of the virus coculture (1 ml) was transmitted to new uninfected MT-2 cells. The cells harvested at the end of each passage were subjected to direct sequencing, and the viral population change was determined by the relative peak height in the sequencing chromatogram. The persistence of the original amino acid substitution was confirmed in all infectious clones used in this assay.

### 2.7. Molecular modeling studies

The programs SYBYL and O were used to prepare models of the complexes of wild-type, M184V, and insertion mutant HIV-1 RT with DNA and the triphosphates of 3TC and EFdA. The starting atomic coordinates of HIV-1 RT were from the structure described by Huang et al. (PDB code 1RTD) (Huang et al., 1998). The side-chain mutations were manually modeled using mostly conformations encountered in RT structures that carry such mutations. The local structures of mutants were optimized using energy minimization protocols in SYBYL. The triphosphates of the inhibitors were built based on the structures of dTTP in

**Table 1**
Antiviral activity against HIV-1 and HIV-2 strains in MT-4 cells

| Compound (abbreviation) | $EC_{50}$ (μM)[a] | | Selectivity[b] | |
|---|---|---|---|---|
| | HIV-$1_{IIIB}$ | HIV-$2_{EHO}$ | $CC_{50}$ (μM)[c] | index |
| 2′-Deoxy-4′-C-ethynyl-adenosine (EdA) | 0.0095 ± 0.0027[d] | 0.006 ± 0.0015 | 104 ± 6.2 | 11,000 |
| 2′-Deoxy-4′-C-ethynyl-2-fluoroadenosine (EFdA) | 0.000073 ± 0.000017 | 0.000098 ± 0.000022 | 9.8 ± 3.4 | 134,000 |
| 2′,3′-Dideoxy-4′-C-ethynyl-2-fluoroadenosine (EFddA) | 1.17 ± 0.29 | 1.07 ± 0.23 | 230 ± 33 | 196 |
| 2′,3′-Didehydro-3′-deoxy-4′-C-ethynyl-2-fluoroadenosine (EFd4A) | 0.11 ± 0.033 | 0.089 ± 0.0007 | 98 ± 26 | 899 |
| 2′-Deoxy-4′-C-cyano-2-fluoroadenosine (CNFdA) | 0.1 ± 0.034 | 0.09 ± 0.0087 | >340 | >3,300 |
| 2′-Deoxy-4′-C-ethynyl-2-chloroadenosine (ECldA) | 0.00069 ± 0.00018 | 0.0006 ± 0.0000028 | 230 ± 16 | 339,000 |
| 2′,3′-Dideoxyinosine (ddI) | 27 ± 12 | 24 ± 4.4 | >100 | >4 |
| 3′-Azido-3′-deoxythymidine (AZT) | 0.0028 ± 0.00062 | 0.0022 ± 0.00073 | 30 ± 7.2 | 10,800 |

Anti-HIV activity was determined by the MTT method.
[a] $EC_{50}$ represents the concentration that blocks HIV-1 replication by 50%.
[b] Selectivity index is calculated by the $CC_{50}/EC_{50}$ for HIV-$1_{IIIB}$.
[c] $CC_{50}$ represents the concentration that suppress the viability of HIV-1-unexposed cells by 50%.
[d] Data shown are mean values with standard deviations for at least three independent experiments.

1RTD, or of tenofovir diphosphate in the ternary complex of HIV-1 RT/DNA/TFV-DP (Tuske et al., 2004).

## 3. Results

### 3.1. Antiviral activity of 4′- and 2-substituted deoxyadenosine analogs

We evaluated the activity of 4′- and 2-substituted deoxyadenosine analogs against HIV-1 with the MTT assay using MT-4 cells. The 2′-deoxy-4′-C-ethynyl nucleoside with adenine as the base (EdA) exerted comparable activity to AZT (Table 1). 2-Fluoro substituted EdA, EFdA, was the most potent against HIV-1 with a sub-nanomolar $EC_{50}$ of 0.073 nM. Selectivity of EFdA and ECldA was much increased compared to parental EdA or AZT. However, EFdA was also relatively cytotoxic compared to other inhibitors of this series. The 2-chloro (Cl) substitution also provided enhanced activity but with a decreased toxicity. Further modifications of the sugar ring from 2′-deoxyribose to 2′,3′-dideoxy- or 2′,3′-didehydro-2′,3′-dideoxy-ribose (EFddA or EFd4A) resulted in a drastic decrease of inhibitory potential. Substitution of the 4′-E group with a structurally similar 4′-cyano group also resulted in markedly decreased inhibitory activity. These results indicate that the 3′-OH and 4′-E moieties in the sugar ring are indispensable for high efficacy, and that antiviral activities are augmented by the modification with F- or Cl-moiety at the adenine 2-position. These compounds suppressed the replication of HIV-2 at comparable levels as HIV-1, consistent with the hypothesis that they act as nucleoside reverse transcriptase inhibitors (De Clercq, 1998).

### 3.2. Antiviral activity against HIV-1 variants resistant to NRTIs

To assess the effect of 4′- and 2-substituted adenosine analogs against drug resistant HIV-1, we generated recombinant infectious clones carrying various NRTI resistant mutations and tested them using the MAGI assay. We found that EdA, EFdA, and ECldA efficiently suppressed many of the viruses resistant to approved NRTI including the multi-drug resistant (MDR) virus, although the 3TC-resistant variant HIV-$1_{M184V}$ and the multi-drug resistant variant HIV-$1_{M41L/T69SSG/T215Y}$ (Winters et al., 1998) showed modestly increased $EC_{50}$ values to these compounds (Table 2). Interestingly, highly active 4′-E analogs, which have 3′-OH such as EFdA or ECldA, were even more effective against the dideoxy-type NRTI resistant variants K65R, L74V, and Q151M complex than they were against WT RT (Table 2). In contrast, 4′-E analogs without 3′-OH (EFddA and EFd4A) were similar or less effective with these resistant variants compared to WT, although the effect seems to be minimal. EFd4A and 2′-deoxy-4′-C-cyano-2-fluoroadenosine (CNFdA) were moderately active against HIV-$1_{WT}$ and HIV-$1_{MDR}$ (Shirasaka et al., 1995), but less active against HIV-$1_{M184V}$. Susceptibility of even the least active EFddA was still in the low micromolar range, but decreased against both HIV-$1_{M184V}$ and HIV-$1_{MDR}$, by 84- and 13-fold, respectively.

### 3.3. Antiviral activity of EFdA against multi-drug resistant clinical isolates

We went on to further characterize EFdA, the most potent compound of the series, against clinical isolates from patients exposed to many anti-AIDS drugs. Five multi-drug resistant strains (HIV-$1_{IVR405}$, HIV-$1_{IVR406}$, HIV-$1_{IVR412}$, HIV-$1_{IVR413}$, and HIV-$1_{A03}$), which contained various drug-resistance mutations in HIV-1 genes (Table 3), were used. These clinical isolates showed high resistance to AZT, 3TC (HIV-$1_{IVR406}$), and ddI (HIV-$1_{IVR412}$). HIV-$1_{IVR415}$ was also a drug-experienced virus but did not have NRTI-resistance mutations and showed no resistance, or less resistance to the NRTIs tested. Hence, it was used as a drug-sensitive HIV-1. Although antiviral activity of EFdA was slightly reduced against HIV-$1_{IVR405, IVR406, IVR412}$ (5.7- to 7.6-fold) compared to HIV-$1_{IVR415}$, the activity was high enough to suppress viral replication. It should be emphasized that EFdA was active against HIV-$1_{IVR406}$, which had the 3TC-resistant M184I substitution.

To evaluate antiviral activity of EFdA to M184V containing isolates in detail, two isolates harboring M184V were used. We used the MAGI assay that directly determines inhibition on a single replication cycle of HIV-1, so that we could eliminate the possible effects of multiple repli-

**Table 2**
Anti HIV-1 activity against drug-resistant infectious clones

| | $EC_{50}$ (μM)[a] | | | | | | | | |
|---|---|---|---|---|---|---|---|---|---|
| | EdA | EFdA | EFddA | EFd4A | CNFdA | EClda | ddI | AZT | 3TC |
| WT | 0.021 | 0.0011 | 1.2 | 0.35 | 0.21 | 0.0064 | 4.1 | 0.015 | 0.71 |
| K65R | 0.0082 | 0.00023 (×0.2) | 1.56 | 0.2 | ND[b] | 0.0017 (×0.3) | ND | 0.0039 (×0.3) | ND |
| L74V | 0.01 | 0.00048 (×0.4) | 2.52 | 0.54 | ND | 0.0015 (×0.2) | 14.6 | 0.019 (×1.3) | ND |
| V75T | 0.0075 | 0.00067 (×0.6) | 9.13 | 0.95 | ND | 0.005 (×0.8) | ND | 0.047 (×3.1) | ND |
| M41L/T215Y | 0.062 | 0.0016 (×1.5) | 6.7 | 1.67 | ND | 0.0065 (×0.1) | ND | 0.12 (×8) | ND |
| M41L/T69SSG/T215Y[c] | 0.18 | 0.0065 (×6) | ND | ND | ND | 0.025 (×4) | 21 | 0.20 (×13) | 9.9 |
| MDR[d] | 0.011 | 0.00074 (×0.7) | 16 | 0.46 | 0.69 | 0.0057 (×0.9) | 40 | 18 (×1200) | 1.1 |
| P119S | 0.018 | 0.00067 (×0.6) | ND | ND | ND | 0.0062 (×1) | ND | 0.0033 (×0.2) | 0.6 |
| T165A | 0.045 | 0.001 (×0.9) | ND | ND | ND | 0.0082 (×1.3) | ND | ND | 0.66 |
| I142V | 0.077 | 0.001 (×0.9) | ND | ND | ND | 0.0062 (×1) | ND | 0.016 (×1) | 0.36 |
| T165R | 0.088 | 0.0016 (×1.5) | ND | ND | ND | 0.012 (×1.9) | ND | 0.011 (×0.7) | 0.28 |
| M184V | 0.088 | 0.0083 (×7.5) | 101 | 6.41 | 1.76 | 0.084 (×13) | ND | 0.0021 (×0.1) | >100 |
| T165R/M184V | 0.6 | 0.014 (×13) | ND | ND | ND | 0.17 (×27) | ND | 0.0053 (×0.4) | >100 |
| I142V/T165R/M184V | 0.81 | 0.023 (×22) | ND | ND | ND | 0.41 (×65) | ND | 0.0076 (×0.5) | >100 |
| T165A/M184V[e] | 0.43 | 0.015 (×14) | ND | ND | ND | 0.16 (×25) | ND | 0.0049 (×0.3) | >100 |
| P119S/T165A/M184V[e] | 0.5 | 0.015 (×14) | ND | ND | ND | 0.20 (×32) | ND | 0.0043 (×0.3) | >100 |

Anti-HIV activity was determined with the MAGI assay.

[a] The data shown are mean values obtained from the results of at least three independent experiments.

[b] ND: not determined.

[c] HIV-1 variant contains T69S substitution and 6-base pair insertions between codons for 69 and 70 (Ser-Gly) with AZT resistant mutations M41L/T215Y (Winters et al., 1998).

[d] Multi-dideoxynucleoside resistant HIV-1 contains mutations (AGT-GGT, SG) in the *pol* region: A62V/V75I/F77L/F116Y/Q151M (Shirasaka et al., 1995).

[e] These variants were reported by Nitanda et al. during induction of Ed4T resistant variants.

cation cycles on measured antiviral activity. In this assay, EFdA effectively suppressed both replication of HIV-$1_{IVR443}$ and HIV-$1_{IVR463}$. Compared to the $EC_{50}$ value for HIV-$1_{WT}$ in Table 2, reduction of the activity was less than 3-fold, suggesting that EFdA suppresses relatively efficiently 3TC-resistant variants with either M184I or M184V mutations.

### 3.4. ADA stability of EFdA

Cellular ADA is known to convert dA to dI through deamination. Phosphorylation of the deaminated dA analogs, *e.g.*, dI, is less efficient, resulting in low conversion of the active triphosphate (TP) form. In order to assess if the activation of these compounds to their TP forms would be affected by the activity of ADA, we tested whether ADA can degrade EdA or EFdA. While EdA was almost completely deaminated after 90 min exposure to ADA, EFdA was not deaminated for up to at least 90 min (Fig. 2). These results indicate that the 2-halo-substitution in EdA confers significant resistance to degradation by ADA.

### 3.5. Phosphorylation of EFdA

Currently available NRTIs need to be converted to the TP form by host cellular kinases before incorporation into newly synthesized proviral DNA. It has been shown that the antiviral effect of NRTIs was reversed by the addition of their physiological counterpart 2′-deoxynucleosides (Bhalla et al., 1990; Mitsuya et al., 1985). To identify the phosphorylation pathway, we examined whether the antiviral activity of EFdA was reversed by the addition of 2′-deoxynucleosides. Surprisingly, the addition of dC decreased the antiviral activity of EFdA in a dose-dependent manner (Fig. 3). In contrast, dT and dG had no effect on the

**Table 3**
Antiviral activity of EFdA against clinical isolates

| Clinical isolates | Amino acid substitutions in the reverse transcriptation | $EC_{50}$ (μM) | | | |
|---|---|---|---|---|---|
| | | AZT | ddI | 3TC | EFdA |
| PBMCs[a] | | | | | |
| IVR405 | M41L/E44D/D67G/V118I/Q151M/L210W/T215Y | 1.76 | 2.45 | 0.55 | 0.0012 |
| IVR406 | M41L/E44D/D67N/V118I/M184I/L210W/T215Y/K219R | 0.64 | 1.46 | >10 | 0.0011 |
| IVR412 | M41L/E44D/V75L/A98S/L210W/T215F | 3.97 | 9.11 | 0.83 | 0.0016 |
| IVR413 | M41L/E44D/D67N/V75L/A98S/V118I/L210W/T215Y/K219R | 1.0 | 2.22 | 1.46 | 0.00021 |
| A03 | M41L/E44D/D67N/L74V/L100I/K103N/V118I/L210W/T215Y | 0.53 | 2.15 | 0.49 | 0.0001 |
| IVR415 | None | 0.0028 | 0.33 | 0.078 | 0.00021 |
| MAGI cells[b] | | | | | |
| IVR443 | I135T/Y181C/M184V | 0.027 | 3.6 | >100 | 0.0031 |
| IVR463 | M41L/E44D/D67N/M184V/H208Y/L210W/T215Y | 0.31 | 7.5 | >100 | 0.0032 |

All assays were performed in triplicate. AZT, ddI, and 3TC were served as a control.

[a] Antiviral activity was determined by the inhibition of p24 antigen production in the culture supernatant.

[b] HeLa-CD4/CCR5-LTR/β-gal cells was used for the MAGI assay.

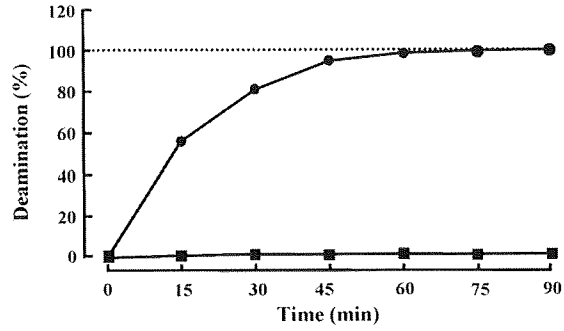


**Fig. 2.** Stability of EFdA following exposure to ADA. EdA or EFdA was incubated with ADA as described in Section 2. The deamination of adenine to inosine was analyzed by HPLC at indicated time points. The data represent the percent of starting compound (EdA; circle, EFdA; box) that was not deaminated by ADA.

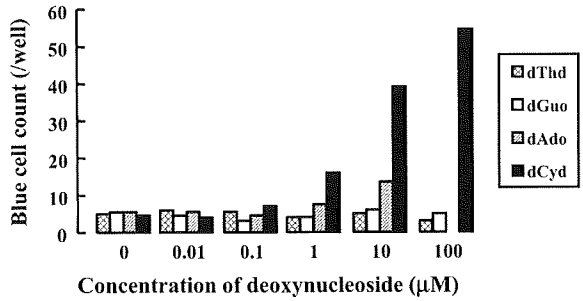


**Fig. 3.** Reversal of the antiviral activity of EFdA in the presence of 2′-deoxynucleosides. Each 2′-deoxynucleoside was added to the medium with serial dilution in the presence of EFdA (3.5 nM). The effect on EFdA activity was determined by the MAGI assay. An ADA inhibitor, dCF, was used during dA competition.

activity of EFdA. We could observe a slight reversal of the antiviral effect by addition of 10 μM dA with dCF. Effect of 100 μM dA could not be examined because of its cytotoxicity. It should be noted that all other tested analogs, including EFddA and EFd4A, were also reversed by the addition of dC (data not shown).

To confirm that the cellular dCK mediates the phosphorylation of EFdA, we examined the antiviral activity of EFdA in the HT-1080, dCK-deficient HT-1080/Ara-C$^r$ (Obata et al., 2001), and dCK-transduced HT-1080/Ara-C$^r$ cell lines. As expected, the antiviral activity of EFdA was markedly reduced in HT-1080/Ara-C$^r$ cells (677-fold), but restored in dCK-transfected cells (Table 4). The same activity profile was observed with ddC, which is also phosphorylated by dCK (Starnes and Cheng, 1987). In contrast, AZT showed comparable activity among three cell lines, since it is known to be phophorylated mainly by thymidine kinase (Furman et al., 1986). Although dCK appears to be the main enzyme responsible for mono-phosphorylation of EFdA, other kinases, such as adenosine/deoxyadenosine kinases, may be partially involved in mono-phosphorylation of EFdA, especially since weak reduction in antiviral activity of EFdA was observed in addition of dA in high concentrations. Moreover, even in dCK-deficient HT-1080/Ara-C$^r$ cells, EFdA exerted moderate antiviral activity. Hence, while it is possible that other kinases may be contributing to a smaller extent to the phosphorylation of EFdA, it appears that dCK is the enzyme that primarily phosphorylates this inhibitor.

### 3.6. Resistance to EFdA

In order to elucidate the mechanism of drug resistance to 4′-E analogs, we selected variants resistant to EdA, a parental compound of EFdA with the dose escalating methods (Nameki et al., 2005). After 58 passages in the presence of EdA, the resistant variants were obtained. Sequence analysis of the entire RT region revealed that a novel combination of mutations, I142V/T165R/M184V was introduced. Similar mutations (I119S/T165A/M184V) were observed in a Ed4T-resistant variant (Nitanda et al., 2005). Hence, we generated infectious clones containing these mutations and tested the antiviral activity of 4′-E analogs against them (Table 2). Mutation in T165, either Arg or Ala, enhanced the resistance against EdA, EFdA, and ECldA in the presence of the M184V mutation. Similar resistance profiles were observed for the I142V/M184V mutations. Furthermore, the triple mutant HIV-$1_{I142V/T165R/M184V}$ had the highest resistance among all tested variants. On the other hand, I142V or T165R alone did not affect the antiviral activity of EFdA or ECldA, although EdA or EFddA showed slightly decreased susceptibility. These results suggest that M184V appears to be the main mutation responsible for 4′-E analog resistance, and the addition of I142V and/or T165R augments the effect of M184V.

### 3.7. Replication of resistant HIV-1

For acquisition of high-level resistance to EFdA as well as EdA, three mutations, I142V, T165R, and M184V were required as described above. To examine the effect of the mutations on the viral replication kinetics we performed an assay that follows production of p24 gag antigen. All clones with M184V showed reduced replication kinetics (Fig. 4A), consistent with the reports that introduction of M184V markedly impairs replication kinetics (Wainberg et al., 1996; Yoshimura et al., 1999). Introduc-

**Table 4**
The effect of dCK expression on the EFdA antiviral activity[a]

| Cell | $EC_{50}$ (μM)[b] | | |
|---|---|---|---|
| | AZT | ddC | EFdA |
| HT-1080 | 0.0032 ± 0.001 | 0.75 ± 0.22 | 0.00031 ± 0.0001 |
| HT-1080/Ara-C$^r$ | 0.0027 ± 0.0005 (0.84) | 84 ± 15 (112) | 0.21 ± 0.03 (677) |
| HT-1080/Ara-C$^r$/dCK | 0.0025 ± 0.00074 (0.78) | 0.51 ± 0.16 (0.68) | 0.000098 ± 0.000034 (0.32) |

[a] SEAP activity in the culture supernatants were determined on day 2 after virus infection.
[b] The data shown are mean ± S.D. and fold increase in $EC_{50}$ compared to HT-1080 is shown in parentheses.

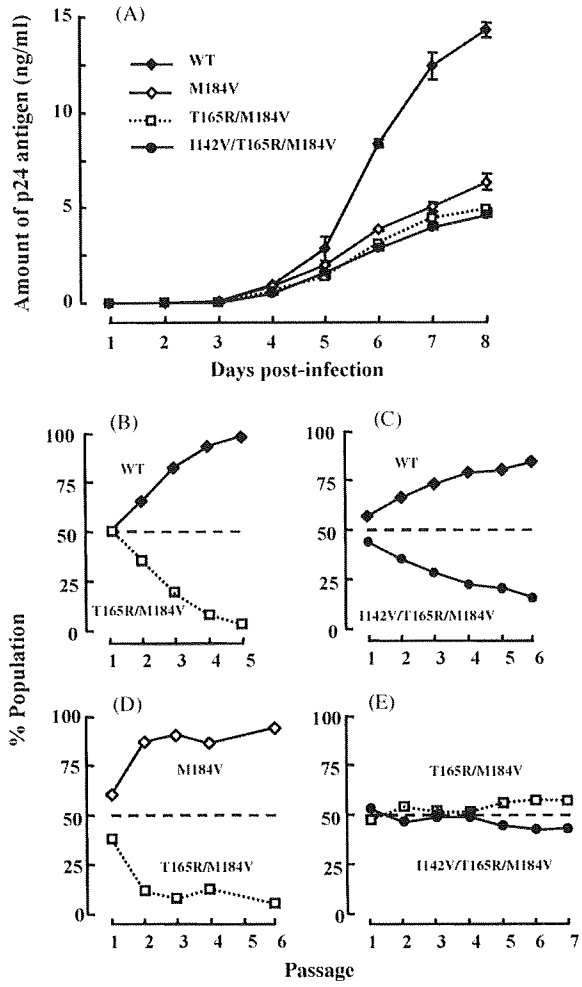


**Fig. 4.** Replication kinetics of HIV-1 clones with mutations. Production of p24 antigen in culture supernatant was determined with a commercially available p24 antigen kit. Profiles of replication kinetics (p24 production) of HIV-$1_{WT}$ (closed diamonds), HIV-$1_{M184V}$ (open diamonds), HIV-$1_{T165R/M184V}$ (open squares with broken line) and HIV-$1_{I142V/T165R/M184V}$ (open circles) were determined with MT-2 (A). Representative results from three independent triplicate determinations of p24 production with newly titrated viruses are shown. MT-2 cells were infected simultaneously with equal amounts of two HIV-1 clones to be compared. At each passage (5–6 days) the proviral sequences were determined and the percent population of each clone is reported at different passage; competition of WT and T165R/M184V (B); competition of WT with I142V/T165R/M184V (C); competition of M184V with T165R/M184V (D), and competition of T165R/M184V with I142V/T165R/M184V (E). At least two independent CHRAs were performed and are shown the representative results.

tion of T165R or I142V/T165R mutations in an M184V background (HIV-$1_{T165R/M184V}$ or HIV-$1_{I142V/T165R/M184V}$, respectively) further impaired HIV replication compared to HIV-$1_{M184V}$. I142V which enhanced EFdA resistance of HIV-$1_{T165R/M184V}$ (Table 2) conferred no replication rescue of HIV-$1_{T165R/M184V}$. To determine detailed replication kinetics, we performed CHRA which compares qualitatively viral replication. As shown in Fig. 4A, HIV-$1_{T165R/M184V}$ and HIV-$1_{I142V/T165R/M184V}$ showed reduced replication kinetics compared to HIV-$1_{WT}$ (Fig. 4B and C). Replication kinetics ofHIV-$1_{I142V/T165R/M184V}$ was comparable to that of HIV-$1_{T165R/M184V}$, which showed further reduced replication kinetics compared to HIV-$1_{M184V}$ (Fig. 4D and E). In another experiment, replication of HIV-$1_{I142V/T165R/M184V}$ was slightly decreased compared to HIV-$1_{T165R/M184V}$ (data not shown). These results suggest that introduction of three EdA mutations that also confers EFdA resistance impaired replication of HIV-1 in much greater extent compared to that of M184V.

## 4. Discussion

At present, HIV-1 variants containing NRTI-resistance mutations are widely observed not only in NRTI-experienced but also in NRTI-naïve patients. In such cases treatment failure is sometimes observed within short periods. The NRTI tenofovir, appears to be more effective against drug-experienced HIV-1 strains (Srinivas and Fridland, 1998). Unlike the other clinically available NRTIs, tenofovir has highly flexible acyclic ribose ring without a 3′-OH. Structural studies have suggested that the compact size of this inhibitor may contribute to the absence of highly resistant mutant strains against tenofovir (Tuske et al., 2004). Despite its unique structural profile, tenofovir is similar to other NRTIs in that it also lacks a 3′-OH group.

In contrast, the highly active 4′-E analogs such as EFdA retain the 3′-OH group of the canonical dNTP substrate. Similar to other NRTIs, they are also phosphorylated by cellular enzymes to their TP active form, which in turn serves as a substrate for HIV RT that incorporates them in an elongating primer during DNA synthesis. Following incorporation, replication is further inhibited by chain termination, although the specific mechanism of chain termination remains to be elucidated. Despite the fact that the 4′-E analogs have a 3′-OH like canonical dNTP substrates, cellular polymerases are likely to discriminate against these analogs, and not incorporate them during cellular DNA polymerization, as suggested by *in vitro* experiments with mitochondrial polymerase γ (Nakata et al., 2007). Alternatively, it is also possible that cellular proofreading systems excise the 4′-E analogs after their incorporation into cellular DNA.

The 3′-OH also plays an important role in phosphorylation of EdA analogs. Based on crystallographic results Sabini et al. reported that the interaction between 3′-OH of nucleosides and catalytic site of dCK was important for efficient nucleoside phosphorylation (Sabini et al., 2003). Alternatively, it is possible that the EFddA and EFd4A nucleosides that lack 3′-OH are poor substrates for HIV RT. The substitution at the 2-position of the purine base is also likely to contribute to highly potent *in vivo* activity of EF- or ECldA, possibly by preventing deamination of the inhibitor by ADA. ADA deaminates the adenine base into inosine, which is a poor substrate for cellular kinases. Similar ADA resistance has been reported for 2′-deoxy-2-chloroadenosine, a chemotherapeutic agent against hairy cell leukemia and chronic lymphocytic leukemia (Carson et al., 1980). ADA resistance may contribute to a longer intracellular half-life for EFdA-TP as compared to that of AZT (Nakata et al., 2007), indicating that substitution of 2-position plays an important role in sustained activity. When CEM cells were exposed to AZT or EFdA at concen-

tration of 0.1 μM, amounts of corresponding intracellular TP-forms were comparable (Nakata et al., 2007). However, inhibitory effect of EFdA in MT-4 and MAGI cells was approximately 40- and 15-fold superior compared to that of AZT (Tables 1 and 2). Taken together, HIV-1 RT appears to preferentially incorporate EFdA-TP compared to AZT-TP, although detailed enzymatic confirmation is needed. The parental EdA also seems to be a good substrate for HIV-1 RT; however, it may be subjected to deamination, resulting in comparable activity to AZT.

There are at least two mechanisms by which HIV RT can become resistant to NRTIs: first, HIV RT can acquire mutations at, or close to the dNTP-binding site, such that help it discriminate against NRTI-triphosphates, while it retains its ability to recognize the normal dNTP substrates (Huang et al., 1998). In the case of M184V/I the discrimination is based on steric conflict between a part of the inhibitor (the sulfur atom of the thioxolane ring in the case of 3TC), and the β-branched side chain of Val or Ile at the mutation site (Sarafianos et al., 1999). Mutations at other residues of the dNTP-binding site are responsible for discrimination of dideoxynucleosides from dNTPs during both the substrate-recognition (Martin et al., 1993) and the catalytic steps (Deval et al., 2002; Selmi et al., 2001). The other mechanism of NRTI resistance is based on an excision reaction (phosphorolysis) that unblocks NRTI-terminated primers using a molecule of ATP as the pyrophosphate donor (Meyer et al., 1999). The product of this reaction is a dinucleoside tetraphosphate and an unblocked primer that can continue viral DNA synthesis. In this case, the role of resistance mutations is to optimize binding of an ATP molecule that is used for the nucleophilic attack at the primer terminus. Most of AZT resistance as well as multi-NRTI resistance of RT with insertions at the fingers subdomain are thought to be based on an ATP-based unblocking mechanism. The insertions in RT destabilize the normally stable ternary complex (RT/template-primer/dNTP) and facilitate the ATP-mediated pyrophospholysis (Boyer et al., 2002). The fingers insertion mutant can excise all nucleotide analogs, with various degrees of efficiency.

Our molecular modeling studies are consistent with a mechanism of resistance to 4′-E analogs that involves steric hindrance between the 4′-E group of the inhibitors and the side chain of V184, reminiscent of the resistance mechanism to 3TC. While a single M184V mutation confers strong resistance to 3TC (>100-fold), it causes only moderate (8- to 13-fold) resistance to EFdA and EClda (Table 2). This is consistent with our molecular modeling analysis where the bulky and rigid 4′-E moiety appears to cause some steric hindrance with the Val or Ile side chain at position 184 during incorporation of the 4′-E nucleotides by the M184V enzyme (Fig. 5). The steric interaction appears to be stronger during incorporation of 3TC-TP (Fig. 5E) than EFdA-TP (Fig. 5C). Interestingly, the M184V mutation appears to confer stronger resistance to 4′-methyl substituted nucleotides, than to the 4′-ethynyl substituted nucleotides (Kodama et al., 2001). The decreased resistance of 4′-ethynyl substituted compounds may be in part the result of compensatory favorable interactions of the longer ethynyl group with residues of the dNTP binding site, including Y115 and D185. Such interactions may moderate the effect of the steric interactions of the 4′-ethynyl with residue V184 in the M184V mutant. Resistance of M184V to dideoxy-derivatives such as EFddA was unexpectedly high (84-fold). Although we cannot explain the detailed mechanism of the difference in resistance, it is possible that the presence of a 3′-OH in the EFdA (but not in the EFddA and EFd4A) results in more stabilizing interactions with residues such as Q151 that compensate for the steric hindrance by M184V (Fig. 5D). Hence, EFddA and EFd4A may be easier to push out of the binding pocket than analogs with a 3′-OH. For stronger resistance to 4′-E-2-halo-dAs, other mutations at positions 142 and 165 in addition to the M184V are required (Table 2) to substantially decrease inhibitor binding. It should be noted that the T165R/M184V mutations were also observed during induction of resistant variants to parental compound EdA. Nitanda et al. also reported that resistant variants for 4′-Ed4T contain M184V with T165A (Nitanda et al., 2005). As shown in Fig. 5A, the effect of the T165R mutation seems to be through the loss of a hydrogen bond between the side chain of Q182 and the side chain OH moiety of T165. Instead, there may be a hydrogen bond between C=O of the main chain of 184 and Q182 in the case of T165R/A, which would affect the positioning of the residue in position 184. Interestingly, HIV-2 has an Arg residue at position 165, whereas HIV-1 has Thr. We could not find decreased susceptibility in HIV-$1_{T165R}$ or HIV-2, indicating that R165 becomes relevant only when Val is at the 184 position. When this residue is Met (T165R in M184 background), resistance is not affected substantially (1.5- to 2-fold resistance, Table 2) because of the flexibility of the Met side chain. However, when the 184 residue is Val (T165R/M184V), the position of 184 may be affected in a way that exacerbates the steric interactions between the ethynyl group of the incoming EFdA and the side chain of V184, resulting in resistance to EFdA and the other 4′-E analogs (13–27-fold resistance, Table 2). At this point it is not clear why the I142V mutation further augmented the effects of M184V and T165R. Finally, as shown in Fig. 5B, there are no apparent substantial steric problems for binding of EFdA to HIV-$1_{M41L/T69SSG/T215Y}$ RT, and the enzyme–inhibitor interactions are likely to be similar to those with dNTP and consistent with the relatively low resistance observed with this variant (Table 2) that is known to cause strong excision-based NRTI resistance. Crystallographic studies with the RT resistant variants complexed with the inhibitors should provide more insights into the mechanism of resistance.

The M184V, one of three mutations associated with EFdA resistance, develops rapidly under therapy with 3TC and has been reported to alter several profiles of RT function, including decreased RT processivity (Back et al., 1996), reduced nucleotide-dependent primer unblocking (Gotte et al., 2000), and increased fidelity (Wainberg et al., 1996). These profiles result in impaired viral fitness, hypersensitivity to other NRTIs, especially AZT (Larder et al., 1995), and delayed appearance of mutations, respectively. Our results show that modest resistance to EdA comes at a significant cost for the virus: The I142V and T165R mutations reduced even further viral replication kinetics of M184V-containing virus. Furthermore, the virus containing these mutations retains the AZT hyper-susceptibility which is induced by

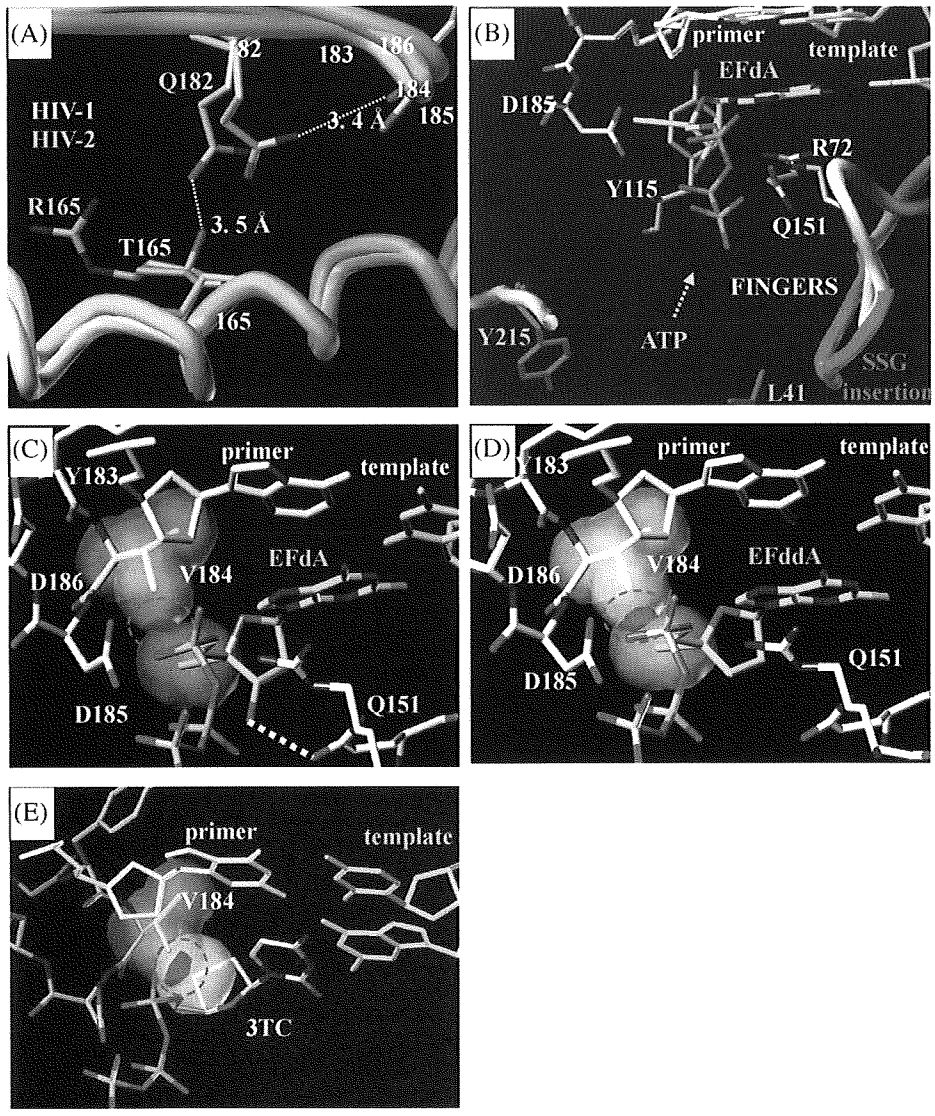


**Fig. 5.** Structural modeling of reverse transcriptase and compounds. (A) Superposition of the polymerase active sites of HIV-1 (gray) and HIV-2 (magenta) reverse transcriptases. Q182 makes a hydrogen bond with T165 in HIV-1. In the T165R mutant of HIV-1, the arginine side chain is expected to have a conformation similar to the one observed for R165 in HIV-2. In this context, Arg does not make a hydrogen bond with the side chain of residue 182 that may now interact with the main chain carbonyl of M184, which is at the immediate vicinity of the inhibitor-binding site. Such interaction may explain how the T165R mutation exacerbates the role of the M184V mutation in resistance to EFdA. (B) Proposed interactions of EFdA-triphosphate (TP) at the polymerase active site of the "fingers-insertion" NRTI-resistant HIV-1 RT, carrying the M41L/T69SSG/T215Y mutations. Possible steric interactions between the 4′-E group of EFdA-TP (C) or EFddA-TP (D) and the sulfur (S) of the pseudosugar ring of 3TC-TP (E). Van der Waals surfaces of 4′-E group (C and D) and S at sugar ring (E) are indicated in green and yellow. Possible steric interactions are shown as overalap of Van der Waal volumes of interacting atoms (in red).

M184V (Table 2), although further experiments are needed. These results suggest that the I142V and T165R mutations simply enhance resistance of M184V RT to EdA rather than optimize the viral fitness of the M184V virus. The increased cost for the virus to overcome inhibition pressure by EdA may have significant clinical benefits in the treatment of HIV infections.

Since EFdA is initially phosphorylated mainly by dCK and its activity was attenuated by addition of dC (data not shown), it is likely that dC analogs, such as 3TC and emtricitabine (FTC) that are mainly phosphorylated by dCK would act as a competitor of EFdA phosphorylation. However, one of dC analogs, apricitabine (ATC) showed little competition for the intracellular phosphorylation of 3TC and FTC (Bethell et al., 2007). Thus, interaction of NRTIs using identical phosphorylation enzymes should be carefully examined.

In conclusion, we have shown that the 2-halogen substituted EdAs have exceptionally potent subnanomolar antiviral activities. The 2-F substituted analog exhibited the highest potency and had a selectivity index significantly improved over that of approved NRTIs. In fact, results from our parallel studies with mice show no toxicity of EFdA (data not shown). The earlier studies also showed that a

parental nucleoside, EdA was not toxic in mice (Kohgo et al., 2004). The half-life of the intracellular TP form of EFdA is substantially extended (~17 h) compared to that of AZT (~3 h) (Nakata et al., 2007), suggesting that it may be possible to administer these inhibitors once a day. Further investigation may lead to their development as potential therapeutics against HIV infections.

## Acknowledgements

We would like to thank S. Oka, T. Sasaki, M. Emerman, J. Overbaugh, K.-T. Jeang, M. Baba for providing HIV-1 clinical isolates, HT-1080 and HT-1080/Ara-C$^r$ cell lines, HeLa-CD4-LTR/β-gal cells and HeLa-CD4/CCR5-LTR/β-gal cells through the AIDS Research and Reference Reagent Program, Division of AIDS, National Institute of Allergy and Infectious Diseases (Bethesda, MD), pNL101, pLTR-SEAP-puro, respectively. A.K. is supported by the 21st Century COE program of the ministry of Education, Culture, Sports, Science, and Technology. This work was supported by a grant for the promotion of AIDS Research from the Ministry of Health, Labor, and Welfare (E.K. and M.M.), a grant for Research for Health Sciences Focusing on Drug Innovation from The Japan Health Sciences Foundation (E.K. and M.M.).

## References

Back NK, Nijhuis M, Keulen W, Boucher CA, Oude Essink BO, van Kuilenburg AB, et al. Reduced replication of 3TC-resistant HIV-1 variants in primary cells due to a processivity defect of the reverse transcriptase enzyme. EMBO J 1996;15(15):4040–9.

Bethell R, De Muys J, Lippens J, Richard A, Hamelin B, Ren C, et al. In vitro interactions between apricitabine and other deoxycytidine analogues. Antimicrob Agents Chemother 2007;51(8):2948–53.

Bhalla KN, Li GR, Grant S, Cole JT, MacLaughlin WW, Volsky DJ. The effect in vitro of 2′-deoxycytidine on the metabolism and cytotoxicity of 2′,3′-dideoxycytidine. AIDS 1990;4(5):427–31.

Boyer PL, Sarafianos SG, Arnold E, Hughes SH. Nucleoside analog resistance caused by insertions in the fingers of human immunodeficiency virus type 1 reverse transcriptase involves ATP-mediated excision. J Virol 2002;76(18):9143–51.

Carson DA, Wasson DB, Kaye J, Ullman B, Martin Jr DW, Robins RK, et al. Deoxycytidine kinase-mediated toxicity of deoxyadenosine analogs toward malignant human lymphoblasts in vitro and toward murine L1210 leukemia in vivo. Proc Natl Acad Sci USA 1980;77(11):6865–9.

De Clercq E. The role of non-nucleoside reverse transcriptase inhibitors (NNRTIs) in the therapy of HIV-1 infection. Antiviral Res 1998;38(3):153–79.

Deval J, Selmi B, Boretto J, Egloff MP, Guerreiro C, Sarfati S, et al. The molecular mechanism of multidrug resistance by the Q151M human immunodeficiency virus type 1 reverse transcriptase and its suppression using alpha-boranophosphate nucleotide analogues. J Biol Chem 2002;277(44):42097–104.

Dutschman GE, Grill SP, Gullen EA, Haraguchi K, Takeda S, Tanaka H, et al. Novel 4′-substituted stavudine analog with improved anti-human immunodeficiency virus activity and decreased cytotoxicity. Antimicrob Agents Chemother 2004;48(5):1640–6.

Furman PA, Fyfe JA, St Clair MH, Weinhold K, Rideout JL, Freeman GA, et al. Phosphorylation of 3′-azido-3′-deoxythymidine and selective interaction of the 5′-triphosphate with human immunodeficiency virus reverse transcriptase. Proc Natl Acad Sci USA 1986;83(21):8333–7.

Gotte M, Arion D, Parniak MA, Wainberg MA. The M184V mutation in the reverse transcriptase of human immunodeficiency virus type 1 impairs rescue of chain-terminated DNA synthesis. J Virol 2000;74(8):3579–85.

Haraguchi K, Takeda S, Tanaka H, Nitanda T, Baba M, Dutschman GE, et al. Synthesis of a highly active new anti-HIV agent 2′,3′-didehydro-3′-deoxy-4′-ethynylthymidine. Bioorg Med Chem Lett 2003;13(21):3775–7.

Huang H, Chopra R, Verdine GL, Harrison SC. Structure of a covalently trapped catalytic complex of HIV-1 reverse transcriptase: implications for drug resistance. Science 1998;282(5394):1669–75.

Jeang KT, Chun R, Lin NH, Gatignol A, Glabe CG, Fan H. In vitro and in vivo binding of human immunodeficiency virus type 1 Tat protein and Sp1 transcription factor. J Virol 1993;67(10):6224–33.

Kajiwara K, Kodama E, Matsuoka M. A novel colorimetric assay for CXCR4 and CCR5 tropic human immunodeficiency viruses. Antivir Chem Chemother 2006;17(4):215–23.

Kimpton J, Emerman M. Detection of replication-competent and pseudotyped human immunodeficiency virus with a sensitive cell line on the basis of activation of an integrated beta-galactosidase gene. J Virol 1992;66(4):2232–9.

Kodama EI, Kohgo S, Kitano K, Machida H, Gatanaga H, Shigeta S, et al. 4′-Ethynyl nucleoside analogs: potent inhibitors of multidrug-resistant human immunodeficiency virus variants in vitro. Antimicrob Agents Chemother 2001;45(5):1539–46.

Kohgo S, Yamada K, Kitano K, Iwai Y, Sakata S, Ashida N, et al. Design, efficient synthesis, and anti-HIV activity of 4′-C-cyano- and 4′-C-ethynyl-2′-deoxy purine nucleosides. Nucleosides Nucleotides Nucleic Acids 2004;23(4):671–90.

Kosalaraksa P, Kavlick MF, Maroun V, Le R, Mitsuya H. Comparative fitness of multi-dideoxynucleoside-resistant human immunodeficiency virus type 1 (HIV-1) in an In vitro competitive HIV-1 replication assay. J Virol 1999;73(7):5356–63.

Larder BA, Kemp SD, Harrigan PR. Potential mechanism for sustained antiretroviral efficacy of AZT-3TC combination therapy. Science 1995;269(5224):696–9.

Little SJ, Holte S, Routy JP, Daar ES, Markowitz M, Collier AC, et al. Antiretroviral-drug resistance among patients recently infected with HIV. N Engl J Med 2002;347(6):385–94.

Martin JL, Wilson JE, Haynes RL, Furman PA. Mechanism of resistance of human immunodeficiency virus type 1 to 2′,3′-dideoxyinosine. Proc Natl Acad Sci USA 1993;90(13):6135–9.

Meyer PR, Matsuura SE, Mian AM, So AG, Scott WA. A mechanism of AZT resistance: an increase in nucleotide-dependent primer unblocking by mutant HIV-1 reverse transcriptase. Mol Cell 1999;4(1):35–43.

Mitsuya H, Weinhold KJ, Furman PA, St Clair MH, Lehrman SN, Gallo RC, et al. 3′-Azido-3′-deoxythymidine (BW A509U): an antiviral agent that inhibits the infectivity and cytopathic effect of human T-lymphotropic virus type III/lymphadenopathy-associated virus in vitro. Proc Natl Acad Sci USA 1985;82(20):7096–100.

Miyake H, Iizawa Y, Baba M. Novel reporter T-cell line highly susceptible to both CCR5- and CXCR4-using human immunodeficiency virus type 1 and its application to drug susceptibility tests. J Clin Microbiol 2003;41(6):2515–21.

Nakata H, Amano M, Koh Y, Kodama E, Yang G, Bailey CM, et al. Activity against Human Immunodeficiency Virus Type 1, intracellular metabolism, and effects on human DNA polymerases of 4′-ethynyl-2-fluoro-2′-deoxyadenosine. Antimicrob Agents Chemother 2007;51(8):2701–8.

Nameki D, Kodama E, Ikeuchi M, Mabuchi N, Otaka A, Tamamura H, et al. Mutations conferring resistance to human immunodeficiency virus type 1 fusion inhibitors are restricted by gp41 and Rev-responsive element functions. J Virol 2005;79(2):764–70.

Nitanda T, Wang X, Kumamoto H, Haraguchi K, Tanaka H, Cheng YC, et al. Anti-human immunodeficiency virus type 1 activity and resistance profile of 2′,3′-didehydro-3′-deoxy-4′-ethynylthymidine in vitro. Antimicrob Agents Chemother 2005;49(8):3355–60.

Obata T, Endo Y, Tanaka M, Uchida H, Matsuda A, Sasaki T. Deletion mutants of human deoxycytidine kinase mRNA in cells resistant to antitumor cytosine nucleosides. Jpn J Cancer Res 2001;92(7):793–8.

Ohrui H. 2′-Deoxy-4′-C-ethynyl-2-fluoroadenosine, a nucleoside reverse transcriptase inhibitor, is highly potent against all human immunodeficiency viruses type 1 and has low toxicity. Chem Rec 2006;6(3):133–43.

Palella Jr FJ, Delaney KM, Moorman AC, Loveless MO, Fuhrer J, Satten GA, et al. Declining morbidity and mortality among patients with advanced human immunodeficiency virus infection. HIV Outpatient Study Investigators. N Engl J Med 1998;338(13):853–60.

Sabini E, Ort S, Monnerjahn C, Konrad M, Lavie A. Structure of human dCK suggests strategies to improve anticancer and antiviral therapy. Nat Struct Biol 2003;10(7):513–9.

Sarafianos SG, Das K, Clark Jr AD, Ding J, Boyer PL, Hughes SH, et al. Lamivudine (3TC) resistance in HIV-1 reverse transcriptase involves steric hindrance with beta-branched amino acids. Proc Natl Acad Sci USA 1999;96(18):10027–32.

Selmi B, Boretto J, Sarfati SR, Guerreiro C, Canard B. Mechanism-based suppression of dideoxynucleotide resistance by K65R human